

# Water Resources Research®



## RESEARCH ARTICLE

10.1029/2021WR029867

### Key Points:

- Snow water equivalent data-assimilation improves hydrologic response in the coupled LIS/WRF-Hydro model for a case study in the Tuolumne River basin
- Horizontal surface routing increases soil moisture and evapotranspiration downstream near channels in LIS/WRF-Hydro, compared to an LSM-only simulation

### Supporting Information:

Supporting Information may be found in the online version of this article.

### Correspondence to:

T. M. Lahmers,  
[timothy.lahmers@nasa.gov](mailto:timothy.lahmers@nasa.gov)

### Citation:

Lahmers, T. M., Kumar, S. V., Rosen, D., Dugger, A., Gochis, D. J., Santanello, J. A., et al. (2022). Assimilation of NASA's Airborne Snow Observatory snow measurements for improved hydrological modeling: A case study enabled by the coupled LIS/WRF-Hydro system. *Water Resources Research*, 58, e2021WR029867. <https://doi.org/10.1029/2021WR029867>

Received 3 MAY 2021  
Accepted 10 MAR 2022

## Assimilation of NASA's Airborne Snow Observatory Snow Measurements for Improved Hydrological Modeling: A Case Study Enabled by the Coupled LIS/WRF-Hydro System

Timothy M. Lahmers<sup>1,2</sup> , Sujay V. Kumar<sup>1</sup> , Daniel Rosen<sup>3</sup> , Aubrey Dugger<sup>4</sup> , David J. Gochis<sup>4</sup> , Joseph A. Santanello<sup>1</sup> , Chandana Gangodagamage<sup>1,2</sup> , and Rocky Dunlap<sup>3</sup>

<sup>1</sup>Hydrological Sciences Lab, NASA Goddard Space Flight Center (NASA-GSFC), Greenbelt, MD, USA, <sup>2</sup>Earth System Science Interdisciplinary Center (ESSIC), University of Maryland, College Park, MD, USA, <sup>3</sup>NOAA/Earth System Research Laboratory, Boulder, CO, USA, <sup>4</sup>National Center for Atmospheric Research, Boulder, CO, USA

**Abstract** The NASA LIS/WRF-Hydro system is a coupled modeling framework that combines the modeling and data assimilation (DA) capabilities of the NASA Land Information System (LIS) with the multi-scale surface hydrological modeling capabilities of the WRF-Hydro model, both of which are widely used in both operations and research. This coupled modeling framework builds on the linkage between land surface models (LSMs), which simulate surface boundary conditions in atmospheric models, and distributed hydrologic models, which simulate horizontal surface and sub-surface flow, adding new land DA capabilities. In the present study, we employ this modeling framework in the Tuolumne River basin in central California. We demonstrate the added value of the assimilation of NASA Airborne Snow Observatory (ASO) snow water equivalent (SWE) estimates in the Tuolumne basin. This analysis is performed in both LIS as an LSM column model and LIS/WRF-Hydro, with hydrologic routing. Results demonstrate that ASO DA in the basin reduced snow bias by as much as 30% from an open-loop (OL) simulation compared to three independent datasets. It also reduces downstream streamflow runoff biases by as much as 40%, and improves streamflow skill scores in both wet and dry years. Analysis of soil moisture and evapotranspiration (ET) also reveals the impacts of hydrologic routing from WRF-Hydro in the simulations, which would otherwise not be resolved in an LSM column model. By demonstrating the beneficial impact of SWE DA on the improving streamflow forecasts, the article outlines the importance of such observational inputs for reservoir operations and related water management applications.

**Plain Language Summary** Land surface models are useful because of their ability to resolve surface-atmosphere feedbacks, including those with vegetation. Land surface models also have the capability to assimilate surface observations, usually measured through remote sensing techniques, into the model. Hydrologic models have the strength of resolving horizontal movements of water both on the surface and through the sub-surface. In the present study, we combine the data-assimilation capabilities of the NASA-LIS land surface model with the WRF-Hydro hydrologic model to combine the utility of both systems. We use this new system to demonstrate the impact of assimilating snow water equivalent, measured from an aircraft, on both the land surface and streamflow from the model in the Tuolumne River basin in Central California. Results show that assimilation of snow water equivalent into the coupled model corrects snow errors and improves the streamflow in both wet and dry years. We find that hydrologic processes that are now added to the land surface model impact simulated soil moisture and evapotranspiration. These findings are important because the ability for a model to better resolve streamflow, from snow assimilation, could be beneficial for water management.

## 1. Introduction

Accurate understanding of the hydrological cycle and the variability of its components is becoming increasingly important for water management, especially in semi-arid environments like the western US. The significant natural heterogeneity and the ubiquitous nature of anthropogenic impacts on the land surface, however, makes it challenging to quantify these complex processes. Detailed representation of the underlying processes through advanced model practices and exploitation of information from remote sensing through methods such as data assimilation (DA) are critical for reducing the uncertainty within global and regional hydrological predictions (Lettenmaier et al., 2015).

© 2022. The Authors.

This is an open access article under the terms of the [Creative Commons Attribution License](https://creativecommons.org/licenses/by/4.0/), which permits use, distribution and reproduction in any medium, provided the original work is properly cited.

Land surface models (LSMs) and hydrological models are two different classes of models that are often used for modeling terrestrial hydrologic processes, but each have a different historical legacy and modeling emphasis (e.g., Clark et al., 2015). The LSM development has been primarily focused on improving representations of vertical surface energy and water flux estimates by incorporating sophisticated parameterizations of vegetation and the root zone (Pitman, 2003; Peters-Lidard et al., 2017). Modern LSMs include multi-layer formulations of the vertical canopy structure for better representations of physical and biological processes related to stomatal control. The LSMs, however, tend to have simplified representations of surface and subsurface hydrological process, particularly processes related to the horizontal transport of water. Most contemporary LSMs are one-dimensional column models that focus on modeling the vertical moisture transport and do not typically include lateral moisture transport formulations (e.g., Maxwell et al., 2011). In addition, most LSMs have shallow subsurface representations where characterization of water table and the effect of groundwater recharge are largely ignored or highly conceptualized. The development of distributed hydrological models (e.g., Hamman et al., 2018; Regan et al., 2020; Sun et al., 2018), on the other hand, has been focused on physically based representations of runoff processes (e.g., Clark et al., 2017), including formulations for 3-d subsurface flow, macropore flow, and surface water flow processes. The representation of land-atmosphere flux processes in these distributed models are often limited as they are largely based on empirical formulations (e.g., Anderson, 1973; Nielsen & Hansen, 1973).

As both LSMs and hydrological models have their strengths and weaknesses in their model formulations, linking these two classes of models enables the exploitation of advances made in both modeling communities. The Weather Research and Forecast (WRF) Hydrologic Model extension (WRF-Hydro) modeling system (Gochis et al., 2020) was designed as an architecture to explicitly enable these linkages. Though the use of data assimilation methods to take advantage of remote sensing information has been growing in the LSM community (Barbu et al., 2014; de Lannoy et al., 2012; Kumar et al., 2008, 2014; Kumar, Jasinski, et al., 2019; Kumar, Mocko, et al., 2019; Reichle et al., 2007; Zaitchik & Rodell, 2009), its application for hydrological models to date has been limited. To further enhance the WRF-Hydro modeling system with the infusion of land remote sensing and data assimilation capabilities, an advanced terrestrial hydrological modeling system combining the NASA Land Information System (LIS; Kumar et al., 2006; Peters-Lidard et al., 2007) and WRF-Hydro has been developed. LIS is an advanced land surface modeling and data assimilation framework, developed to enable fine-scale land surface modeling and the assimilation of terrestrial hydrology and land surface remote sensing observations. The combination of these DA capabilities with a hydrologic modeling system makes the integrated environment novel.

This article describes the application of the coupled LIS/WRF-Hydro system over the Tuolumne River basin in central California, focusing on the use of remotely sensed snow estimates for DA and the impact of lateral flow on the LSM realized through the hydrological model. Specifically, we employ the coupled system to utilize the high-resolution snow water equivalent (SWE) estimates from NASA's Airborne Snow Observatory (ASO; <https://www.jpl.nasa.gov/missions/airborne-snow-observatory-aso/>) over the Tuolumne River basin in central California. Through DA tools, the ASO SWE estimates are employed to improve the realization of snow states. The impact of improved snow simulation on streamflow simulation is then quantified. The study thus focuses on the following specific science questions:

1. What is the added utility of remotely sensed ASO SWE estimates for improving land surface and hydrologic states, including streamflow?
2. What are the impacts of additional physical processes realized by WRF-Hydro on LSM variables related to the basin hydrologic response?

This article also describes the details of the coupled LIS/WRF-Hydro model. The coupled environment is enabled through the use of the Earth System Modeling Framework (ESMF; Hill et al., 2004), which is a high-performance and flexible approach for coupling Earth system models. The ESMF-based design allows for the clear separation of major modeling system components of LIS and WRF-Hydro and allows for their independent development, while maintaining the integrated modeling environment.

In Section 2 of this paper, we discuss the LIS and WRF-Hydro model structures and the coupling for LIS/WRF-Hydro. Section 3 includes a description of the ASO data set and the LIS/DA methods. In Section 4, we discuss the results from the coupled LIS/WRF-Hydro simulations, impact of the assimilation of ASO data on

streamflow, and the added impact of hydrologic routing on land surface states. Section 5 includes a summary and main conclusions of this work.

## 2. LIS/WRF-Hydro Model Description

### 2.1. LIS Structure and Configuration

LIS is an open source land surface modeling and data assimilation framework that supports modeling over user-specified regional or global domains using an ensemble of LSMs. LIS permits high-resolution LSM simulations and the multivariate and concurrent assimilation of terrestrial remote sensing datasets. The DA subsystem in LIS is an interoperable environment that supports both sequential and non-sequential assimilation approaches such as the Ensemble Kalman Filter (EnKF), particle Filter (pF), and the Ensemble Kalman Smoother (EnKS). These algorithms can be employed with a large suite of observational inputs and LSMs within LIS. In the present study, we take advantage of LIS's data assimilation subsystem within the coupled LIS/WRF-Hydro environment to assimilate NASA ASO SWE estimates over the upper Tuolumne basin (described in Section 3.4 below). The LIS capabilities have been demonstrated for the assimilation of a wide range of remote sensing datasets including soil moisture (e.g., Kumar et al., 2008, 2009; Peters-Lidard et al., 2011), snow (Kumar et al., 2014; Kumar, Peters-Lidard, Arsenault, et al., 2015; Liu et al., 2013, 2015), skin temperature (Reichle et al., 2010), terrestrial water storage (Kumar et al., 2016), vegetation (Kumar, Jasinski, et al., 2019; Kumar, Mocko, et al., 2019) and albedo (e.g., Kumar et al., 2020).

### 2.2. WRF-Hydro Structure and Configuration

The WRF-Hydro model can be coupled to the WRF Advanced Research WRF (WRF-ARW) atmospheric model or executed offline as a stand-alone hydrologic simulation. In this study we are running WRF-Hydro in its “stand-alone” configuration coupled to LIS and not to an atmospheric model. The NOAA National Water Model (NWM) operational hydrologic model is based on the WRF-Hydro model architecture (e.g., Lahmers et al., 2019, 2021), and WRF-Hydro has also been used for research in land-atmosphere interactions (e.g., Arnault et al., 2016). WRF-Hydro (Gochis et al., 2020) can be implemented with either the Noah (Ek et al., 2003) or Noah-MP LSMs (Niu et al., 2011) to resolve vertical soil processes and exchanges with the atmosphere. In addition to the LSM, WRF-Hydro includes horizontal overland and subsurface flow on a high-resolution terrain routing grid. Surface overland flow uses diffusive wave routing (Julien et al., 1995; Ogden, 1997). Shallow saturated sub-surface flow (i.e., within the 2-m LSM soil column) is also resolved within the high-resolution routing grid of WRF-Hydro using a Boussinesq approximation. In the present study, WRF-Hydro is configured with a 250-m routing grid, similar to the NWM configuration of WRF-Hydro. WRF-Hydro uses a conceptual baseflow model to resolve deep groundwater flow. Water that drains out of the bottom of the LSM soil column is aggregated over the drainage area for a specific reach, then stored and slowly released to the channel using an exponential model based on stored water depth. Our LIS/WRF-Hydro configuration uses the gridded diffusive wave channel flow routing option of WRF-Hydro.

WRF-Hydro has been used for both research and operations. The NOAA National Weather Service (NWS) Office of Water Prediction (NWS/OWP) uses WRF-Hydro as the model architecture for the NWM to produce nationwide streamflow, soil moisture, snow, and ET forecasts (e.g., Gochis et al., 2020). WRF-Hydro has also been tested and modified for a range of local-scale and coupled land-atmosphere studies (e.g., Arnault et al., 2016; Lahmers et al., 2020).

### 2.3. LIS/WRF-Hydro Model Coupling

As noted earlier, the integrated LIS/WRF-Hydro system is developed using the standardized software tools and paradigms enabled by ESMF. Prior to coupling of these systems, both LIS and WRF-Hydro were made ESMF compliant, and these updates will carry through subsequent model versions. ESMF includes a superstructure for enveloping model and coupler components and an infrastructure of commonly used utilities, including grid transformations, time management, and data communications. The ESMF design accommodates a wide range of data structures, data discretizations, and component layout and sequencing options. Explicit, semi-implicit,

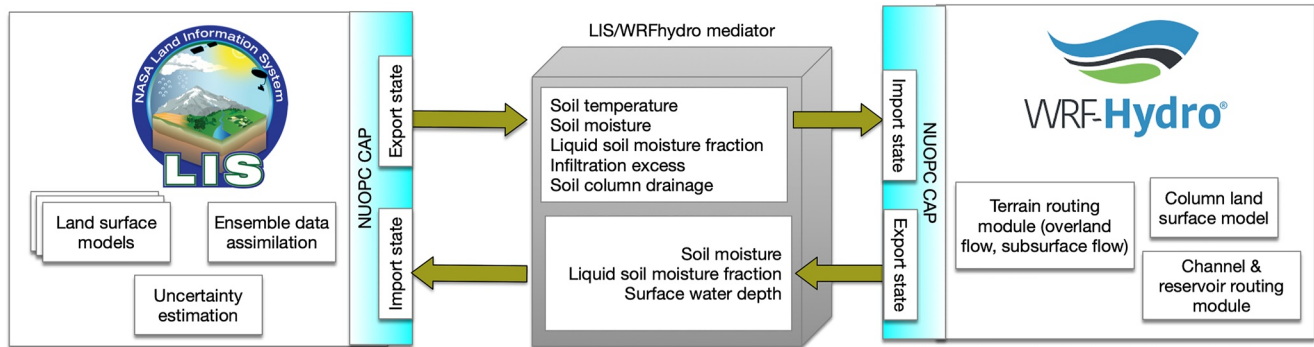


**Figure 1.** Conceptual illustration of the LIS/WRF-Hydro system. LIS and WRF-Hydro share data through a mediator in the center of the image that exchanges model variables through the LIS and WRF-Hydro NUOPC caps.

and implicit coupling interactions that involve 2- and 3-dimensional, regional/global, logically rectangular, point cloud and mesh grid types are supported by ESMF. The coupled LIS/WRF-Hydro environment also uses a recent enhancement to ESMF called the National Unified Operational Prediction Capability (NUOPC; Theurich, 2014), which provides coupling protocols for building, initializing, and sequencing models that enable rapid transition and increased interoperability between ESMF-based modeling systems. The interoperability between model components is ensured through the implementation of a NUOPC interface or “cap”, which can be reused across modeling systems.

NUOPC provides generic representations of four key modeling system elements: (a) A NUOPC model is a wrapper around the geophysical model code that provides a standard interface to the model data and execution subroutines, (b) a NUOPC driver controls the execution of a set of child components based on a user-defined run sequence, (c) a NUOPC mediator contains custom code for coupling, flux computations, spatial and temporal transforms and other data manipulations and (d) a NUOPC connector that implements standard communication options such as redistribution of data across different numbers of processors and grid remapping using various interpolation methods. The LIS/WRF-Hydro system utilizes NUOPC driver, connector, mediator, and model components to exchange data between an ensemble of coupled land surface and hydrological models. The use of NUOPC standardizes component interfaces and interoperability while preserving model integrity. This software architecture is illustrated in Figure 1, and it enables LIS/WRF-Hydro to run on high performance computing (HPC) environments from a single executable file. LIS/WRF-Hydro in the present study uses Noah-MP version 4.0.1, which is called through the LIS framework. The coupled configuration is as close as possible to WRF-Hydro as a standalone model and has been tested to verify this consistency.

Figure 1 also shows the different software components of LIS/WRF-Hydro. The coupled system adds NUOPC caps to both LIS and WRF-Hydro. These caps enable the models to pass variables to and from a mediator. Thus LIS, which calls the Noah-MP v4.0.1 LSM, and WRF-Hydro are separately called by the main driver at timesteps set by the user. The LIS and WRF-Hydro structures then exchange variables through a LIS/WRF-Hydro mediator. For example, LIS executes first and then passes a set of exchange variables to the mediator. Then the mediator redistributes or interpolates data from the LIS domain to the WRF-Hydro domain. The data are then passed to WRF-Hydro before WRF-Hydro executes, and this same process occurs in reverse when WRF-Hydro feedback variables are returned to LIS. The LIS/WRF-Hydro mediator also supports an ensemble of LIS and WRF-Hydro coupled instances, which enables ensemble DA instances.

The DA subsystem within LIS executes the land surface model in an ensemble mode, with small perturbations applied to a select set of model states and meteorological fields. This land surface model ensemble exists entirely within one instance of LIS. At this time a single instance of WRF-Hydro does not support an ensemble of hydrological model instances. In order to avoid coupling an ensemble of land surface model instances to a single hydrological model instance, the LIS/WRF-Hydro system and LIS/WRF-Hydro mediator support running multiple instances of one model in a single executable (i.e., WRF-Hydro). This allows for each member of the LIS ensemble to couple to an individual instance of WRF-Hydro. The LIS/WRF-Hydro mediator redistributes or interpolates data to each hydrological model from the ensemble of land surface model instances. Conversely, data



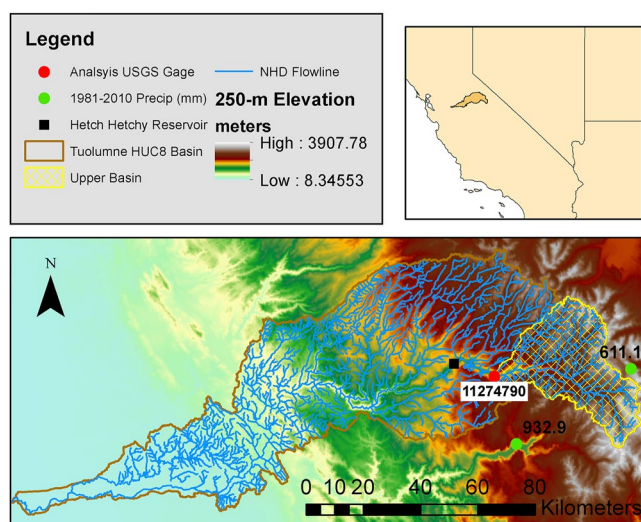


**Figure 2.** The Tuolumne test basin is shown relative to the Contiguous US (CONUS) (top). The full basin with National Hydrography Data set (NHD) flowlines is shown in the bottom panel. The Upper Tuolumne Basin analysis area with the analysis USGS Gage, Hetch Hetchy Reservoir, elevation from the 250-m grid, and two precipitation observations are also shown.

from each WRF-Hydro instance is gathered in the LIS/WRF-Hydro mediator before it is returned to the LIS model. The result is a single executable capable of running an ensemble of coupled model instances.

### 3. Datasets and Methodology

#### 3.1. NASA Airborne Snow Observatory (ASO) Estimates

The NASA ASO SWE data set is obtained from an observation platform that combines a scanning lidar and an imaging spectrometer to measure snow depth and albedo (Painter et al., 2016). ASO data were measured in approximately weekly intervals over the Tuolumne River Basin during the cold season, and the full data set consists of SWE, depth, and snow albedo. SWE and snow depth are assimilated in the present study; however, albedo is not considered. These variables are assimilated at 00 UTC on the days they are available. SWE is of principal focus of this study, as it is used in our DA system (described in detail in Section 3.3). The ASO data set has a 50-m resolution and its use of high-density Lidar measurements permits it to resolve small-scale variability in snow properties that cannot be resolved by coarser datasets or point estimates. Note that since ASO SWE is derived from snow depth using in situ measurements and model-based assumptions on spatially distributed snow density, more uncertainty in the derived ASO SWE (compared to snow depth) is likely.

ASO has been used in several other recent studies for snow verification and hydrologic modeling. Henn et al. (2016) demonstrated that ASO data, when fused with streamflow for model calibration, was able to reduce the uncertainty of inferred precipitation in a catchment with limited precipitation observations. Cao et al. (2018) used Variable Infiltration Capacity (VIC) LSM combined with ASO to estimate SWE in the Tuolumne basin and used this data set to validate two satellite based snow products. Oaida et al. (2019) used ASO data to validate a high-resolution SWE data set based on DA of Moderate Resolution Imaging Spectroradiometer (MODIS) snow data (Painter et al., 2009) into the VIC hydrologic model. This recent work with ASO demonstrates its potential use for hydrologic simulations and possible benefits when integrated with LIS/WRF-Hydro.

#### 3.2. Evaluation Datasets

For evaluation of LIS and LIS/WRF-Hydro SWE, three reference data products are considered: (a) the University of Arizona (UA; Dawson et al., 2016), (b) the Snow Data Assimilation System (SNODAS; Barrett, 2003), and (c) California Cooperative Observing Sensors (California COOP sites; available at <http://cdec.water.ca.gov/>). These grid and point observations are considered over the upper basin study area shown in Figure 2, which is fully encompassed by the ASO observation area. The University of Arizona data set is based on gridded upscaled point measurements of snow (~4-km resolution) computed using piecewise linear regression of point measurements and topography (Dawson et al., 2016). The SNODAS data set uses a snow model that is forced with numerical weather prediction (NWP) data and updated through DA of remote sensing snow observations daily (~1-km resolution). The California COOP sites consist of snow pillow measurements maintained by the state of California.

We acknowledge that the SNODAS and University of Arizona gridded datasets have coarser resolution than the ASO model products. Though the two gridded datasets are also developed by incorporating observational data products within a model, evaluation of LIS and LIS/WRF-Hydro compared to these products is still a benchmark for improvement from DA compared to the open-loop simulations, since these datasets are independent of the ASO product. These limitations of the gridded datasets are also the reason why the California COOP sites are also considered where available.

Streamflow is validated using USGS streamflow measurements at a single gage above Hetch Hetchy Reservoir. USGS maintains hourly streamflow at sites throughout the CONUS (available online at: <https://waterdata.usgs.gov/nwis/rt>). Details of the gage used in the study area are discussed in Section 3.4.

**Table 1**  
*LIS and LIS/WRF-Hydro Simulation Descriptions*

Simulation Name	Description
LIS-OL	LIS Noah-MP v4.0.1 model run without assimilation
LIS-DA	LIS Noah-MP v4.0.1 with ASO SWE DA
LIS/WRF-Hydro-OL	LIS Noah-MP v4.0.1 coupled to WRF-Hydro, including surface routing, sub-surface flow, baseflow, and channel routing without assimilation
LIS/WRF-Hydro-DA	LIS Noah-MP v4.0.1 coupled to WRF-Hydro, including surface routing, sub-surface flow, baseflow, and channel routing with ASO SWE DA

### 3.3. Model Configuration

We consider the impacts of physical processes realized through both DA and hydrologic routing by executing four different model simulations for the same Tuolumne basin domain (see next section) as a multi-year case study that includes both wet and dry winters. Atmospheric forcing data sets needed to execute LIS and LIS/WRF-Hydro include incoming shortwave radiation, incoming longwave radiation, specific humidity, air temperature, surface pressure, and near surface wind (both  $u$  and  $v$  components). The model is forced with atmospheric variables and precipitation from version 2 of the North American Land Data Assimilation System (NLDAS-2) forcing data set (Xia et al., 2012). We acknowledge that it is possible for the NLDAS-2 product to miss some of the fine-scale precipitation and precipitation variability due to its coarser resolution relative to that of the models and hydrological processes of the region.

LIS was executed for WY2014–2017 with WY2012–2013 as spin-up, and LIS was executed both with and without DA (i.e., LIS-Open Loop (OL) and LIS-DA, respectively). Similarly, LIS/WRF-Hydro was also spun-up for WY2012–2013 and analyzed from WY2014–2017 both without and with DA (i.e., LIS/WRF-Hydro OL and LIS/WRF-Hydro DA, respectively). LIS/WRF-Hydro had identical LSM settings to LIS, but also included horizontal surface and sub-surface flow, channel routing, and baseflow as discussed in Section 2.2. The descriptions of each model simulation are also included in Table 1.

### 3.4. LIS/WRF-Hydro Domain

For the present study, LIS/WRF-Hydro is executed for the full Tuolumne River basin to its outlet with the San Joaquin River (Figure 2); however, our analysis is above the Hetch Hetchy Reservoir (Figure 2). The analysis area in the upper basin has no management of the streamflow and is fully encompassed by the ASO data set. Note that the ASO data set covers slightly more of the Tuolumne basin than just the upper basin above Hetch Hetchy; however, we limit our analysis area to this domain to make analysis of modeled versus measured streamflow possible. Figure 2 also shows the high terrain above Hetch Hetchy reservoir. The precipitation climatology (based on the 1980–2009 NLDAS-2 1/8 Degree precipitation climatology (not shown)) consists of amounts on the order of 800–1,000 mm/yr over much of the basin. 1981–2010 average precipitation is of a similar order of magnitude and shown at two National Weather Service weather stations in Figure 2. While this demonstrates that NLDAS-2 precipitation is comparable to observations, we caution that both the NLDAS-2 and station observations likely underestimate orographic precipitation and are therefore biased toward lower elevations. The upper basin that is used for analysis has a majority of the deciduous broadleaf forests and needleleaf evergreens, with a few small areas of shrublands.

The 1-km LSM grid for the full model used in the present study was derived using Land surface Data Toolkit (LDT; Arsenault et al., 2018), which is the preprocessing environment for LIS. The 250-m WRF-Hydro routing grid, channel grid, and the baseflow basin model grid was derived using version 5.1.1 of the WRF-Hydro GIS Pre-Processing tools (Sampson & Gochis, 2020) based on the Hydrosheds (Available online at: [https://www.hydrosheds.org/images/inpages/HydroSHEDS\\_TechDoc\\_v1\\_2.pdf](https://www.hydrosheds.org/images/inpages/HydroSHEDS_TechDoc_v1_2.pdf)) digital elevation model (DEM) data set. The baseflow basin model grids, as described above, were derived using the default ‘FullDom LINKID local basins’ method of the WRF-Hydro processing tools (Sampson & Gochis, 2020), where groundwater basins are derived for specific channel reaches (computed from the routing grid). All model parameters are default values based on Noah-MP and WRF-Hydro parameter lookup tables, and no model calibration was performed.

### 3.5. LIS-DA Methods

In the present study, we use a one-dimensional ensemble Kalman Filter (EnKF; e.g., Reichle et al., 2002) for the assimilation of the ASO SWE (Figure 1). As noted in prior studies (Hain et al., 2012; Houtekamer and Mitchell, 1998; Kumar et al., 2008; Pan & Wood, 2006; Reichle et al., 2002; Zhou et al., 2006) EnKF allows for the flexible characterization of model errors with an ensemble and the handling of non-linear model dynamics and temporal observational discontinuities. Alternative DA approaches such as the Particle Smoothing Approach (e.g., Margulis et al., 2019) offer advantages over EnKF because they can produce analysis results with coarser temporal resolution without discontinuities at assimilation timesteps. These methods are not feasible in the present study, as they require a larger ensemble and have a higher latency window between observations, which is not ideal for hydrologic forecasting applications. The EnKF approach works in a sequential manner by alternating between a model forecast step and an analysis update step.

The forecast step (i.e., running the LSM) is performed first, wherein the analysis state from timestep  $k-1$  is projected forward from  $(\hat{x}_{k-1}^+)$  to the LSM state at  $k$  ( $\hat{x}_k^-$ ). This is followed by the analysis step where the increments are computed as:

$$\hat{x}_k^+ = \hat{x}_k^- + \mathbf{K}_k (\hat{y}_k - \mathbf{H}_k \hat{x}_k^-)$$

where the observation state ( $\hat{y}_k$ ) is combined with the a priori state ( $\hat{x}_k^-$ ) to generate the a posteriori state ( $\hat{x}_k^+$ ).  $\mathbf{H}_k$  represents the observation operator that relates the model states to the observation, and  $\mathbf{K}_k$  is the Kalman gain that acts as the weighting factor that determines the influence of forecast innovations ( $\hat{y}_k - \mathbf{H}_k \hat{x}_k^-$ ) in the analysis update. The Kalman gain is diagnosed as a function of the model error covariance ( $\mathbf{P}_k$ ) and the observational error covariance ( $\mathbf{R}_k$ ).

$$\mathbf{K}_k = \frac{\mathbf{P}_k \mathbf{H}_k^T}{\mathbf{H}_k \mathbf{P}_k \mathbf{H}_k^T + \mathbf{R}_k}$$

Consistent with prior snow studies (e.g., Liu et al., 2015), we use a 20-member ensemble in the present study.

It should be noted that the ensemble assimilation systems are limited when the model spread is insufficient to represent the underlying uncertainty. For example, if the observation represents a non-zero snow value when the model simulation is near zero, developing a reliable ensemble spread to represent the model uncertainty is difficult. These issues are common to all ensemble data assimilation systems as discussed in Kumar et al. (2017) and are not limited to EnKF assimilation.

Noah-MP snow states are computed using a full energy-balance (e.g., accounting of radiative, thermal and liquid mass transport fluxes), multilayer snow model (up to 3 layers) that accounts for changes in snow volume caused by melt and snowfall, as well as changes to density caused by compaction. No explicit accounting for impurities such as dust, black carbon, forest litter or aerosol deposition is made. The snow energy balance is used to estimate snowmelt, sublimation, evaporation and temperature. The top most layer of the snowpack is thinnest and used to compute sensible and latent fluxes as well as radiative exchanges with the atmosphere (Niu et al., 2011). The model state vector in the assimilation consists of the total SWE and snow depth variables. After every data assimilation update, the total SWE is used to update the multilayer snowpack states of Noah-MP. A 20-member ensemble with small perturbations applied to a select set of meteorological forcing variables and the model state vector is used in the present study. The details of the perturbation parameters are shown in Table 2. These settings were recommended by prior experiments (Peters-Lidard et al., 2011; Su et al., 2011) and have been used widely for snow assimilation in recent work (e.g., Kumar et al., 2014; Kumar, Peters-Lidard, Santanello, et al., 2015; Liu et al., 2013, 2015). While strictly speaking, EnKF assumes a linear system with mutually and serially uncorrected associated Gaussian errors (Nerini et al., 2019), such conditions are seldom met in real applications such as the example in this manuscript. The perturbation settings used here are developed from prior studies that ensure a reasonable compromise between the assimilation improvements and possible suboptimal filter performance due to the deviations from Gaussian assumptions (e.g., Crow & Van Loon, 2006; de Lannoy et al., 2012; Kumar et al., 2008; Reichle et al., 2008). Perturbation frequencies for forcing, model state, and observations are set to 1-hour, 3-hours, and 6-hours, respectively. As noted in Liu et al. (2013), perturbations to meteorology forcing, which include cross correlation in space and time, are intended to simulate model uncertainty for DA. Time correlation uses a first-order regressive model (time-order of 3-hours) as in Liu et al. (2013). In order to avoid the

**Table 2**  
*Parameters for Meteorological Forcing and Model State Variables for EnKF Configuration*

Variable	Perturbation Type	Std. Dev.	Cross Correlation across variables			
			SW corr	LW corr	PCP corr	T corr
Meteorological Forcing						
Downward Shortwave (SW)	Multiplicative	0.2	1	−0.3	−0.5	0.3
Downward Longwave (LW)	Additive	30	−0.3	1	0.5	0.6
Precipitation (PCP)	Multiplicative	0.5	−0.5	0.5	1	−0.1
Near surface Air Temperature (T)	Additive	0.5	0.3	0.6	−0.1	1
Noah LSM snow states			SWE	snod		
SWE	Multiplicative	0.01	1	0.9		
Snow depth (snod)	Multiplicative	0.01	0.9	1		

addition of spurious skill in the model ensemble from perturbations, a bias correction approach following Ryu et al. (2009) is employed.

## 4. Results

### 4.1. Impacts of ASO DA on LIS and LIS/WRF-Hydro SWE

In this section, we evaluate the impacts of SWE DA in a fully coupled hydrological environment on both direct (SWE) and downstream (ET and soil moisture) variables. The results in Table 3 show that the assimilation of

**Table 3**  
*LIS and LIS/WRF-Hydro Skill Scores Compared to University of Arizona and SNODAS Data on the Top Two Panels and the California COOP Sites on the Bottom Three Panels*

UA	LIS-OL	LIS-DA	LIS/WRF-Hydro OL	LIS/WRF-Hydro DA
RMSE	108.6 (104.9–112.7)	90.9 (87.8–94.4)	108.6 (104.8–112.7)	91.0 (87.8–94.4)
Bias (mm)	−46.9 ± 5.0	−32.5 ± 4.4	−46.8 ± 5.0	−32.5 ± 4.4
R (−)	0.988 (0.987–0.990)	0.980 (0.978–0.982)	0.988 (0.987–0.989)	0.980 (0.978–0.982)
SNODAS				
RMSE	129.3 (124.8–134.1)	99.6 (96.1–103.3)	129.3 (124.7–134.1)	99.6 (96.1–103.4)
Bias (mm)	−49.0 ± 6.1	−34.6 ± 4.8	−48.9 ± 6.1	−34.6 ± 4.8
R(−)	0.980 (0.978–0.982)	0.981 (0.979–0.983)	0.980 (0.978–0.982)	0.981 (0.979–0.983)
DAN CA Coop.				
RMSE	94.6 (91.3–98.2)	169.3 (163.4–175.7)	94.6 (91.3–98.2)	169.4 (163.4–175.7)
Bias (mm)	−31.1 ± 4.6	4.6 ± 8.7	−31.1 ± 4.6	4.6 ± 8.7
R(−)	0.972 (0.969–0.974)	0.893 (0.882–0.903)	0.972 (0.969–0.974)	0.893 (0.882–0.903)
SLI CA Coop.				
RMSE	413.6 (399.1–429.1)	281.8 (271.9–292.4)	413.7 (399.3–429.3)	281.9 (272.0–292.5)
Bias (mm)	−238.3 ± 29.8	−179.5 ± 19.1	−238.3 ± 29.8	−179.6 ± 19.1
R(−)	0.993 (0.993–0.994)	0.978 (0.976–0.980)	0.993 (0.993–0.994)	0.978 (0.976–0.980)
TUM CA Coop.				
RMSE	107.1 (103.3–111.1)	74.7 (77.5–72.1)	107.2 (103.4–111.2)	74.71 (77.5–72.1)
Bias (mm)	−2.8 ± 7.8	−11.3 ± 5.4	−2.8 ± 7.8	−11.3 ± 5.4
R(−)	0.960 (0.955–0.963)	0.982 (0.980–0.984)	0.960 (0.955–0.963)	0.982 (0.980–0.984)

*Note.* For gridded datasets, skill is computed in the basin area above Hetch Hetchy Reservoir. Confidence intervals for RMSE and Bias are based on a Chi-Square Distribution and a student's *t*-test, respectively, for the timeseries of area averaged errors. Intervals are computed for correlation coefficient use a Fisher transform.



ASO SWE results in reduced errors in the snow states in the model. Relative to the respective OL integrations, the LIS-DA and LIS/WRF-Hydro DA simulations have statistically significant reduced RMSE and bias estimates when validated against the University of Arizona data set based on a Chi-Square Distribution and a student's *t*-test (95% confidence intervals for each value are shown), respectively. In particular, the model integrations without assimilation have large negative biases in SWE, but these biases are reduced in both the LIS-DA and LIS/WRF-Hydro-DA simulations compared to the SNODAS and UA datasets. The DA simulations do have slightly worse correlation coefficients (95% confidence intervals are computed using a Fisher transform), likely due to removal of snow in the lower basin (which we will show in later figures). Reductions of negative bias are well pronounced compared to the independent SNODAS and University of Arizona (on the order of ~15%) data sets.

The spatial impact of these results (averaged over the full WY2014–2017 analysis period) is presented in Figure 3, which shows model SWE from the LIS/WRF-Hydro-OL and LIS/WRF-Hydro-DA simulations as well as the reference products (SNODAS and University of Arizona). This figure only shows the upper basin, where ASO snow data are available and that are upstream of the Hetch Hetchy reservoir (Figure 2). Figure 3d shows that LIS/WRF-Hydro in the OL configuration has a less spatially variable distribution of SWE across the domain compared to the DA solution (Fig. 3e), which has more SWE in the high elevation headwater reaches. Both solutions have less snow compared to the two evaluation products (Figures 3a and 3b); however, the DA solution increases the amount of model SWE by as much as 60% in some locations in the higher elevations of the ASO domain (Figure 3f). Lower elevation SWE in the DA solution is decreased. Figure 3c shows the magnitude of these snow increases as well as their relative distribution across the basin. The SWE in the DA solution is more realistic than the OL solution when compared to the independent SNODAS and University of Arizona observations. These improvements in the model SWE are visible despite the tendency for both evaluation datasets to underestimate SWE variations as a function of elevation (discussed in detail in Section 3.2).

The LIS/WRF-Hydro solutions are also compared in Figure 4 at three California Cooperative Snow Measurement Sites (Figure 4a). The DAN site (Figure 4b) has the most complete data, and the bias at this site is clearly reduced from DA. A delay in snowmelt in WY2017 from the DA solution increases RMSE here (Table 3), despite improvements at other times. Observation data at the SLI (Figure 4c) and TUM (Figure 4d) sites are less complete; however, Figure 4 shows the added value of DA, particularly for reducing bias. At these sites, RMSE significantly improves from DA (Table 3), and bias improves at the SLI site. Analysis of Figure 4 and the skill scores from Table 3 show the added value of DA compared to snow observations, in addition to the improvements from the University of Arizona and SNODAS sites.

The impacts of DA can be better understood in Figure 5, which shows the timeseries of the basin average SWE for LIS/WRF-Hydro-OL and LIS/WRF-Hydro-DA for the Tuolumne basin above Hetch Hetchy reservoir as well as all of the observation-based data products. WY2014–2015 were associated with drier than average precipitation due to an ongoing drought, while WY2016–2017 both experienced Atmospheric River events and were associated with wetter conditions. This figure shows that DA generally reduces the low bias of the LIS/WRF-Hydro-OL simulation in both wet and dry years. Changes to the SWE bias are also not uniform in time. For example, LIS/WRF-Hydro-OL has less low bias in WY2014 (Figure 5b) and WY2015 (Figure 5b), both dry years, and LIS/WRF-Hydro-DA is associated with fewer changes to LIS/WRF-Hydro SWE. Meanwhile, low bias in WY2016 (Figure 5c) and WY2017 (Figure 5d; both wet years) is more noticeable, and LIS/WRF-Hydro DA experiences a greater correction. These changes in SWE subsequently impact the streamflow in later timesteps, and the location of SWE changes also impact hydrologic response, both of which are shown in later figures.

Figure 5 also shows that DA causes the model to exhibit some discontinuities in the SWE timeseries. The discontinuities in Figure 5 are a result of the infrequent set of observations and the fact that we are using a sequential data assimilation method. The magnitude of the corrections introduced by DA is dependent on the differences between the observations and the prior model state (before the analysis), which is why the corrections look more dramatic in some years.

Changes to SWE model skill for the full WY2014–2017 analysis period, including RMSE and correlation coefficient, for LIS/WRF-Hydro-OL and LIS/WRF-Hydro-DA are shown in Figure 6. In this figure, correlation and RMSE differences shown in the panels are based on the quantities computed from the timeseries of the model variables compared to the observations at each grid point. This figure includes statistical significance to RMSE changes (based on a Chi-Squared Distribution) and correlation changes (based on a Fisher transform).

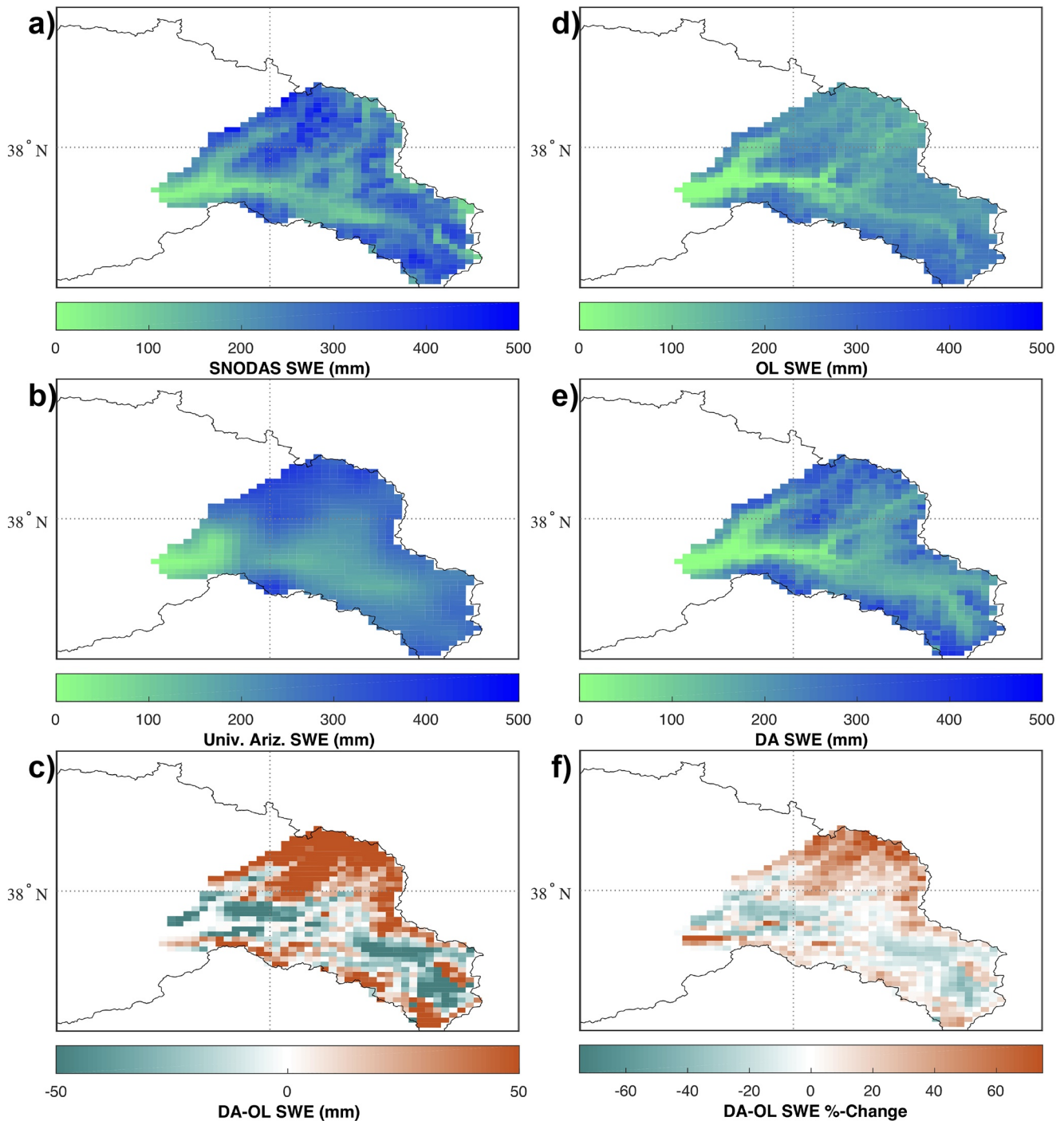


**Figure 3.** Mean SWE (in mm) for SNODAS, (a), University of Arizona (b), LIS/WRF-Hydro DA versus OL (c), LIS/WRF-Hydro OL (d), LIS/WRF-Hydro DA (e) and LIS/WRF-Hydro DA versus OL percent change (f).

DA reduces RMSE, primarily due to decreases in negative bias, across the northern areas of the basin compared to both SNODAS (Figure 6a) and UA SWE (Figure 6c) products. RMSE changes are less consistent in the lower basin, as removal of excess valley snow has a more mixed impact. Even as RMSE is improved over much of the basin due to improvements from bias (particularly in the northern headwaters), there are also areas with increased RMSE (i.e., more error), and these are statistically significant. These increases to RMSE follow decreased correlation coefficients in some of the lower reaches where there is less snow after DA (Figures 3b and 3d). The likely

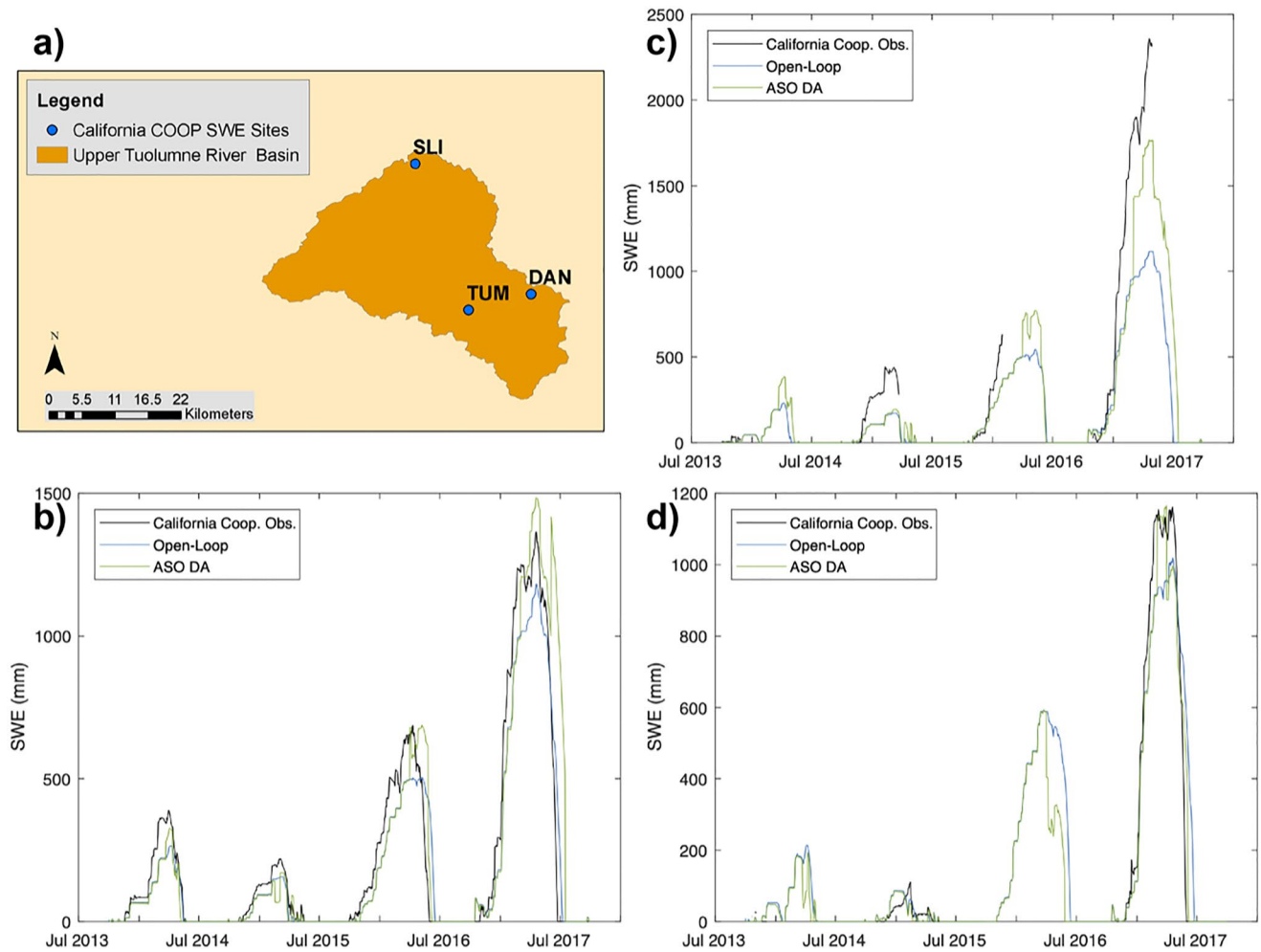


**Figure 4.** California Cooperative SWE sites (a) and LIS/WRF-Hydro OL and LIS/WRF-Hydro DA SWE v. California Cooperative Site SWE. Sites include DAN (b), SLI, (c), and TUM (d).

reason for this reduced model skill is the reduction of SWE in the lower basin may be responsible for reducing the correlation coefficient for SWE in this area due to snow becoming less frequent and therefore more variable. Reductions to model SWE after DA also increase negative bias further upstream to the East, which lead to increased RMSE values. Thus, while DA mostly improves SWE skill, this is not true everywhere in the domain.

Figure 7 shows the impacts of DA on other surface variables in the LIS/WRF-Hydro simulations for the melt season (when surface runoff and streamflow are high). This includes the months of April through July during the full WY2014–2017 period. This figure shows that the northern basin, where DA increases snow, is also associated with increased soil moisture, while soil moisture is reduced slightly downstream (Figures 7a and 7c). This is consistent with the changes to SWE demonstrated in Figures 3c and 3f. While the percent change to snow is large throughout the domain (~50% or greater in some areas; Figure 3f), this corresponds to only minor and often spatially variable changes in ET, even during the melting season (Figures 7b and 7d). These results demonstrate that SWE DA does impact other surface variables, and this is particularly noticeable for soil moisture. While lateral flow routing is more physically consistent with hydrologic systems, the addition of this component does make ET changes from SWE DA more spatially variable.

#### 4.2. Impacts of DA on Streamflow

In this section, we consider the impacts of physical changes realized through ASO SWE DA on streamflow. The only USGS gauge in the upper Tuolumne basin is USGS 11274790, and this is upstream of the Hetch Hetchy

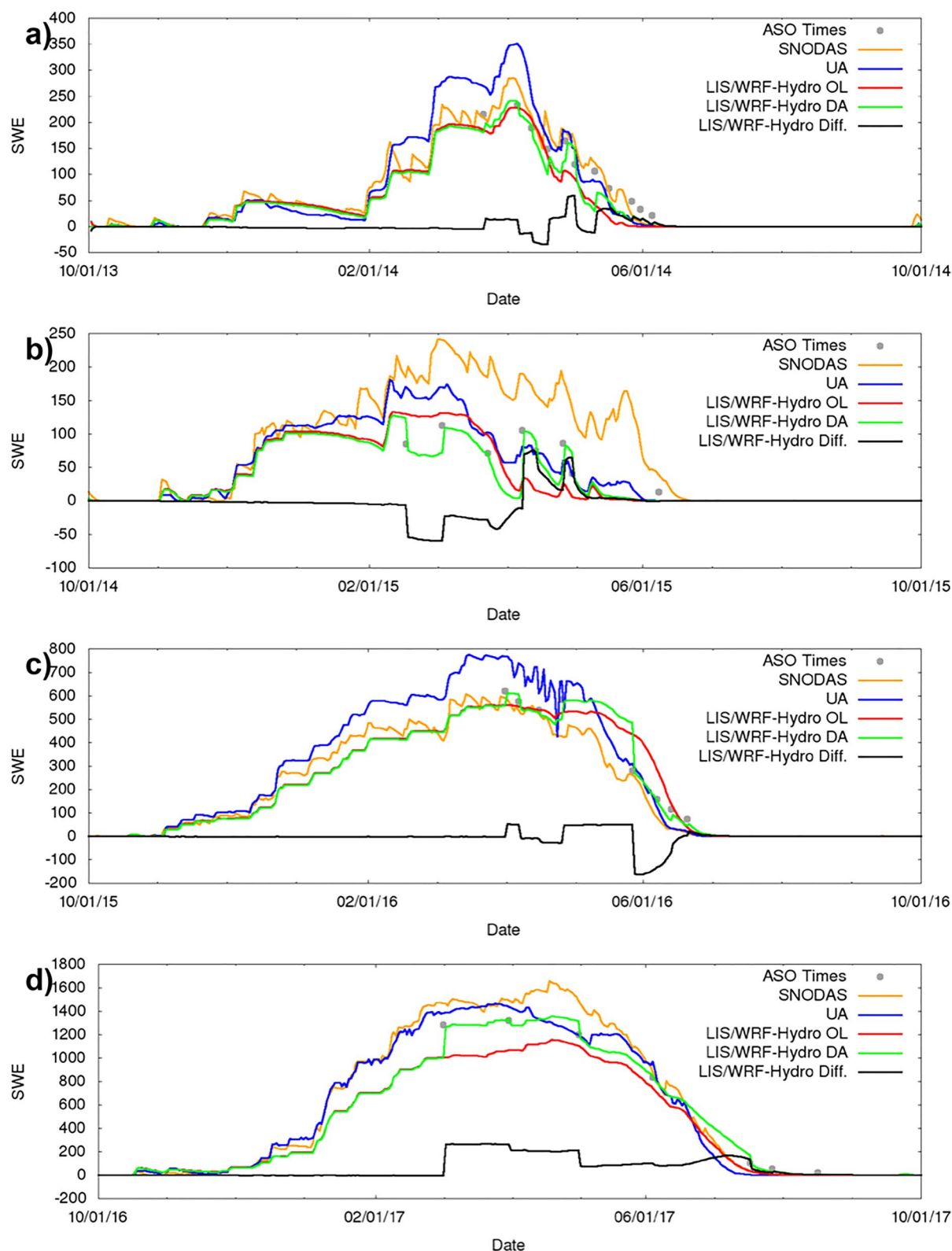


**Figure 5.** Timeseries of modeled (LIS/WRF-Hydro) and observed basin-averaged SWE. Data for WY2014 (top) to WY2017 (bottom).



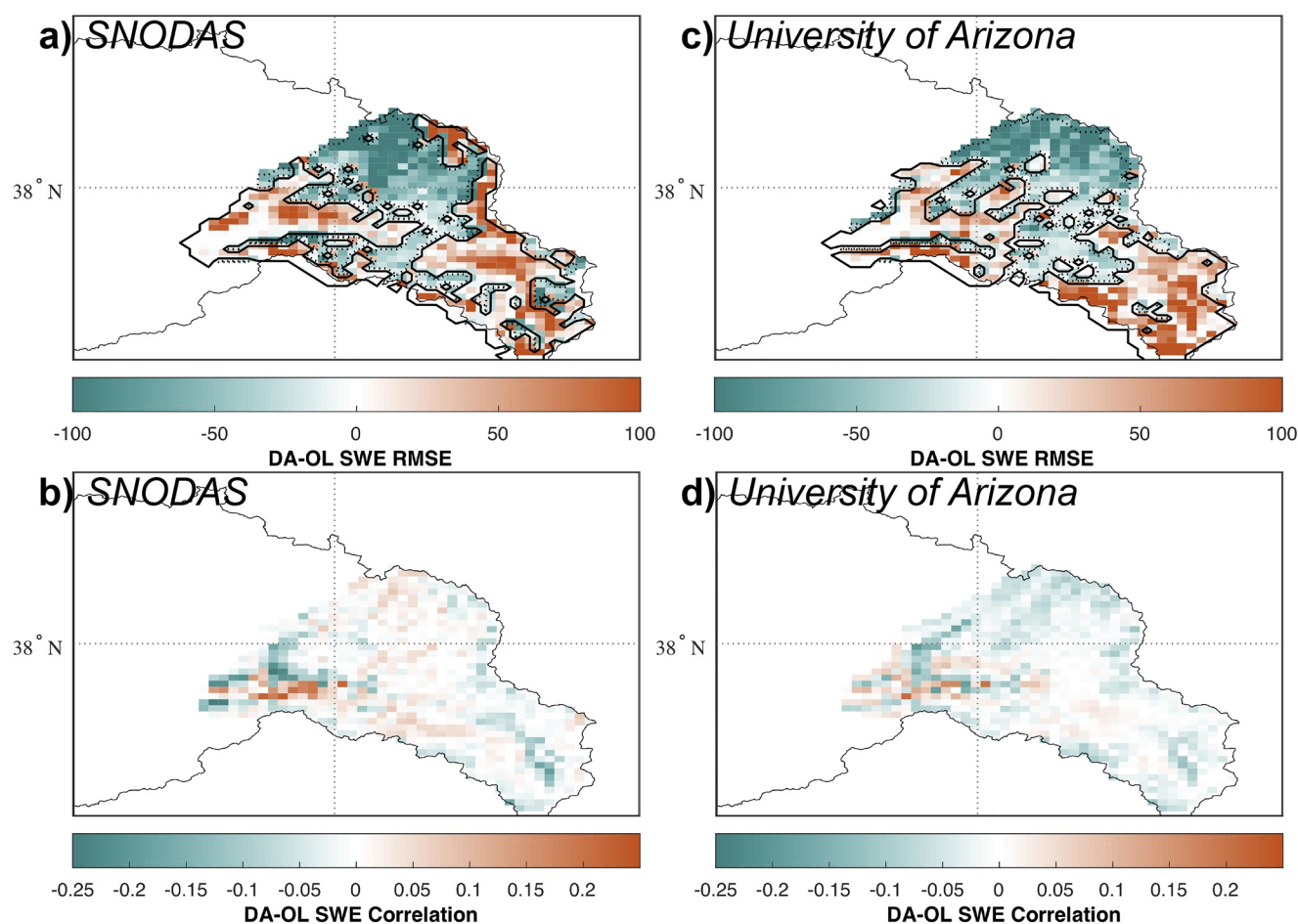


**Figure 6.** Change in RMSE (mm) (top) and Correlation (bottom) from DA compared to SNODAS (left) and University of Arizona observations (right) for the LIS/WRF-Hydro simulations.

reservoir (Figure 2), which significantly alters the hydrologic response downstream for water management. Since this model configuration does not include the reservoir or streamflow extractions/diversions in the lower basin, model streamflow estimates at this gauge are considered “natural” flows and expected to approximate the gage observations in the upper basin only. In this basin, default model parameters are used in WRF-Hydro, so the impacts of calibration are not considered here. Streamflow from the upper basin is shown in Figure 8. Overall, the model hydrologic response reasonably follows the observations, despite the model having a slightly over-active diurnal cycle (where runoff tends to follow snowmelt during the primary melt season due to the diurnal temperature cycle).

For WY2014 (Figure 8a) and WY2015 (Figure 8b), when the basin was drier, SWE DA eliminates some slight low streamflow bias during those dry years, even as water was removed from the snowpack at times during those same years (Figures 5a and 5b). As we will show in later figures, this is due to the redistribution of SWE from DA that can be visualized in Figure 3. Similarly, snow DA substantially decreases wet bias for streamflow during WY2016 (Figure 8c), and to a lesser extent WY2017 (Figure 8d), which were both wetter than the earlier years in the simulation (Figures 5c and 5d). Table 4 shows streamflow skill for both the OL and DA simulations as bias, correlation, RMSE, Nash-Sutcliffe Efficiency (NSE), and Kling-Gupta Efficiency (KGE; Gupta et al., 2009). These quantities are improved from DA. Note that KGE equally weights correlation, bias, and standard deviation errors, while NSE tends to weight correlation higher (e.g., Gupta et al., 2009). This suggests that the changes to snow in the model, which had only nominal changes to SWE in dry years and reduced the low SWE bias in wet years are also able to ameliorate some streamflow biases. During WY2015, LIS/WRF-Hydro with DA is able to capture runoff early in the season that the OL simulation does not resolve. Note that DA only was used for SWE



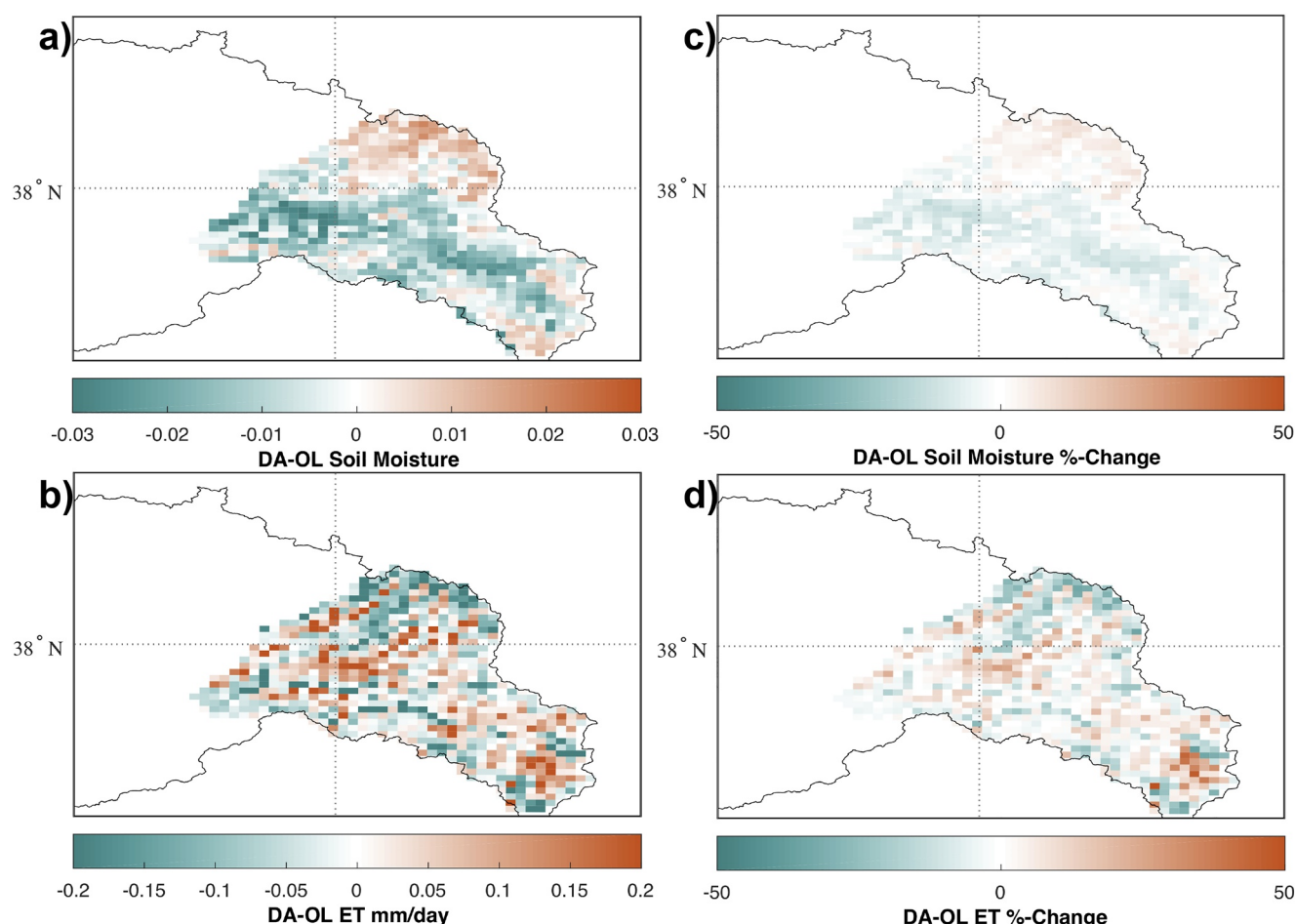


**Figure 7.** Change in Noah-MP 0–10 cm soil volumetric water content (top) and ET (bottom) from ASO DA for LIS/WRF-Hydro (left) and for LIS/WRF-Hydro as a percent change (right) during the snowmelt season (April – July).

(not streamflow or other hydrologic variables); however, these results show added value from snow DA in LIS in a hydrologic simulation.

The physical processes that lead to the redistribution of streamflow due to DA are considered in Figures 9 and 10. In Figure 9, it is obvious that most lateral flow (i.e., surface runoff and shallow saturated flow that reaches the WRF-Hydro channel network) originates in the high elevations, where the snowpack is the greatest. Close analysis of this figure also reveals that much of the flow entering the channel network originates at a few points while inflow in surrounding channel grid points is less. This would be expected in a basin dominated by snow hydrology, and is especially true in the years with greater snowpack (i.e., WY2016–2017). However, Figure 10 also demonstrates that changes to this runoff entering the channels from DA tend to vary in wet and dry years. During dry years (i.e., WY2014–2015), runoff is added to upstream reaches in the northern part of the basin, where SWE is generally the highest (i.e., Figure 3), and this is consistent with the reduction of low streamflow bias during these same years (i.e., Figure 8) from added SWE in these areas. Meanwhile, during the wet years, while some runoff is again added in the high elevation reaches, runoff is also reduced in the lower reaches, consistent with Figure 3 where SWE is reduced in these areas. This reduction of snowpack in the lower basin (above Hetch Hetchy reservoir) is the reason why the high streamflow bias in the OL simulation is reduced in the DA simulation during WY2016–2017. Thus, the spatial redistribution of SWE from DA, where SWE increases in the high elevations but decreases further down seems to be important for correcting some of the model streamflow errors, such that low flow bias during dry years and high flow bias during wet years are partially corrected by these spatial changes that are realized through DA. While the increase in SWE and decrease of streamflow

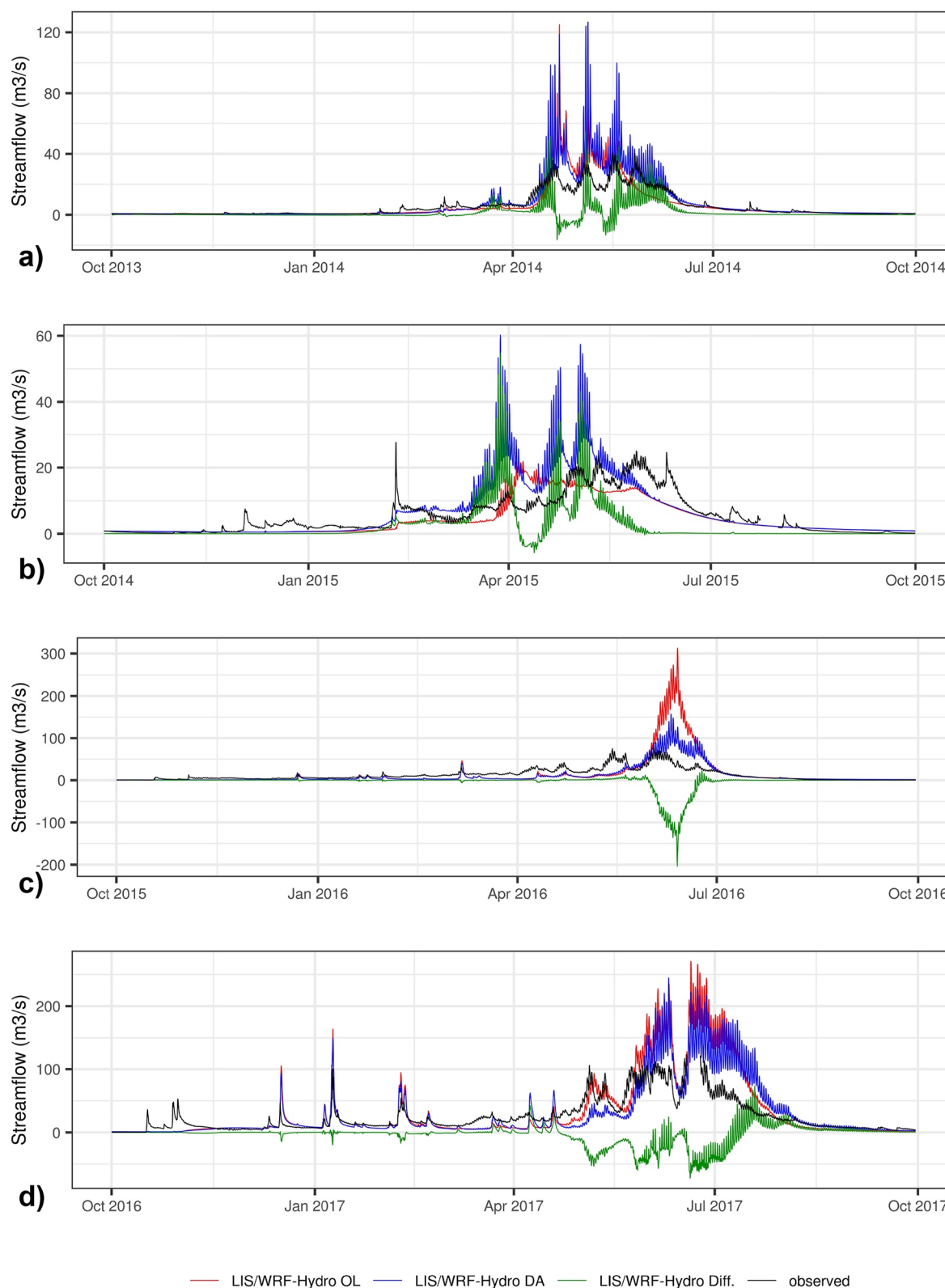


**Figure 8.** Hydrographs from LIS/WRF-Hydro OL (red), LIS/WRF-Hydro DA ensemble mean (dark blue), LIS/WRF-Hydro DA ensemble mean minus OL (green), and observations (black) at USGS gauge 11274790 for WY2014 through WY2017 (top to bottom).

**Table 4**

*Streamflow Skill Scores at USGS Gauge 11274790 for the LIS/WRF-Hydro OL (Control) and LIS/WRF-Hydro DA Ensemble Mean Simulations*

LIS/WRF-Hydro OL Simulation					
Gage	KGE	NSE	Bias	R	RMSE
11274790	0.04	−0.65	15.86	0.80	21.99
LIS/WRF-Hydro DA Simulation					
Gage	KGE	NSE	Bias	R	RMSE
11274790	0.44	0.14	9.48	0.80	15.88

during wet years may seem counter-intuitive, it is consistent with the impact of SWE redistribution on the model hydrologic response.

Figure 10 also shows that DA affects at least some snowmelt and runoff outside of the analysis area above Hetch Hetchy. This is because the ASO domain is slightly larger than our analysis domain. ASO DA does not affect other parts of the basin, as the 1-D EnKF only affects model variables where ASO data are available.

### 4.3. Impacts of Hydrologic Routing on Land Surface States

The coupled LIS/WRF-Hydro system not only enables the translation of improved land surface states through LIS from data assimilation to streamflow, but also allows the simulation of the impact of hydrologic routing on land surface states. In this section, we consider the impacts of that lateral redistribution of water from WRF-Hydro on soil moisture and ET. For example, surface flow recycled from routing that is otherwise removed from the

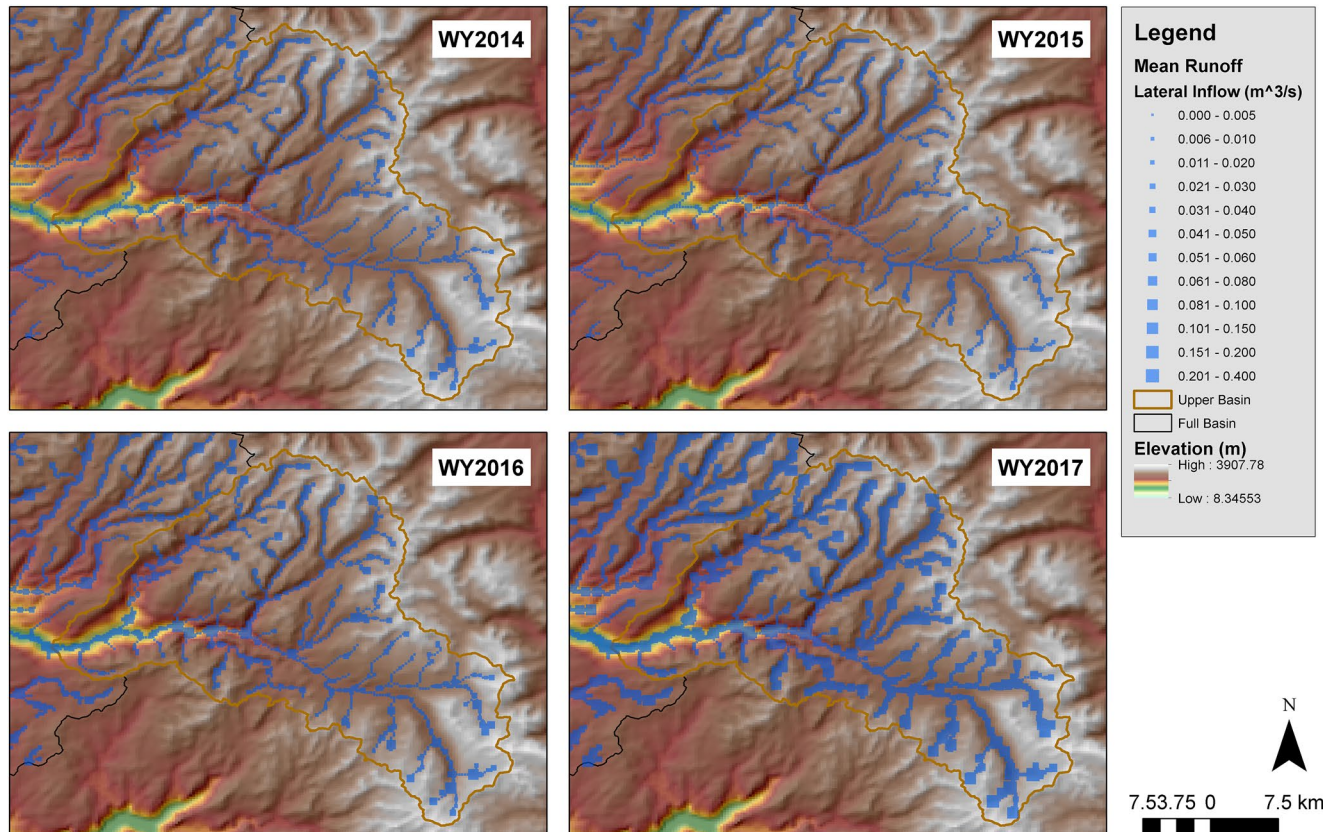


**Figure 9.** Upper Tuolumne Basin mean annual lateral flow ( $\text{m}^3\text{s}^{-1}$ ) into stream channels for WY2014 (top left), WY2015 (top right), WY2016 (bottom left), and WY2017 (bottom right) from the LIS/WRF-Hydro DA simulation.



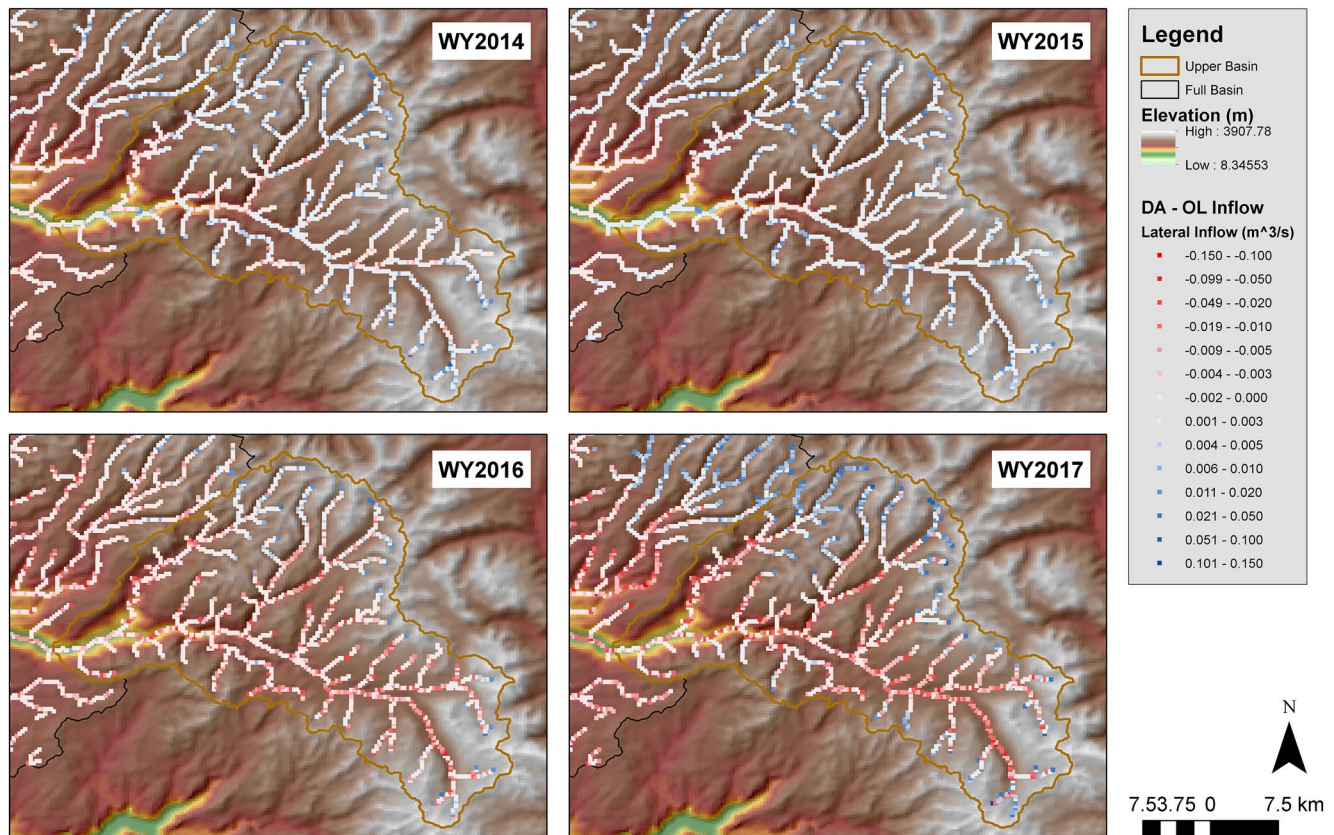


**Figure 10.** Upper Tuolumne Basin DA minus OL change to mean annual lateral flow ( $\text{m}^3\text{s}^{-1}$ ) into stream channels for WY2014 (top left), WY2015 (top right), WY2016 (bottom left), and WY2017 (bottom right).

LSM would influence the soil moisture states (e.g., Lahmers et al., 2020). The influence of the two-way feedbacks simulated by the coupled LIS/WRF-Hydro environment is examined by contrasting the LIS/WRF-Hydro simulations with LIS-only simulations in Supporting Information S1, Figures 11 and 12, and in Table 5.

A figure equivalent to Figure 8 is included in Supporting Information S1, and it considers the impacts of hydrologic model routing by plotting WRF-Hydro channel flow compared to LIS-only surface and sub-surface runoff (the LIS surface runoff variable is not used when coupled to WRF-Hydro terrain routing schemes since explicit routing is included). In this figure, the LIS/WRF-Hydro OL and DA streamflow is plotted with solid red and dark blue lines, respectively (as in Figure 8). LIS OL and DA aggregated surface and sub-surface runoff (over the same basin) are plotted with dashed orange and purple lines, respectively. Observed streamflow is plotted with a solid black line. 24-hour averages are used in this figure as the LIS-only runoff is written daily in our configuration. The LIS-only runoff follows a similar trajectory to LIS/WRF-Hydro, but tends to miss the timing of some peaks captured by LIS/WRF-Hydro and USGS streamflow. LIS-only simulations tend to have runoff peaks that are too fast and flashier compared to the observations and LIS/WRF-Hydro solution. This is especially true earlier in the water year, when runoff is driven by rainfall rather than snowmelt. This is likely due to WRF-Hydro aggregating some runoff and routing it downstream, which is slower and more consistent with the actual hydrologic response. In some cases late in the season, LIS-only runoff (surface and sub-surface) also has a longer recession, which may indicate increased reliance on sub-surface flow. Thus, this figure shows the added value of LIS/WRF-Hydro surface runoff.

The addition of lateral terrain routing tends to influence the hydrologic response, as shown in soil moisture for both the OL (Figure 11a) and DA (Figure 11c) simulations. Figures 11b and 11d shows a vectorized version of the LIS/WRF-Hydro routing grid in the analysis domain. This figure shows that soil moisture changes from routing are relatively constant across much of the model domain, but increases tend to be more pronounced near channel grid cells. As DA reduced SWE and soil moisture further downstream but increased both variables upstream (i.e.,

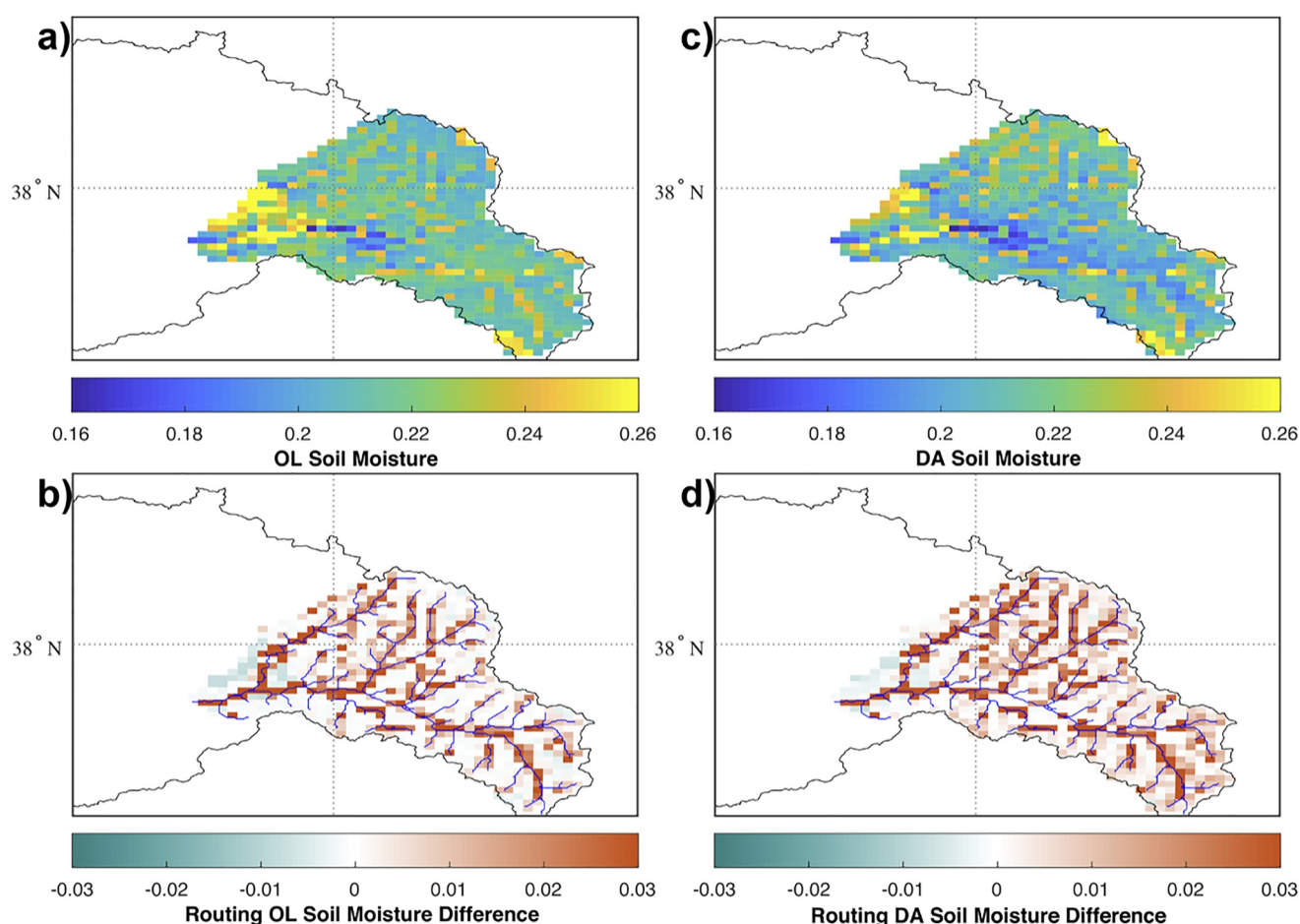


**Figure 11.** Average soil volumetric water content for LIS/WRF-Hydro (top) and change in soil moisture in LIS/WRF-Hydro compared to LIS (bottom) for the OL (left) and DA (right) simulations.

Figures 3 and 7, respectively), the effects of routing are slightly more noticeable downstream when DA is used because lateral terrain routing increases soil moisture downstream in areas where DA would otherwise reduce it. Meanwhile, increases in soil moisture also lead to increased ET near the channel network in LIS/WRF-Hydro (Figures 12b and 12d). Basin ET averages are also shown in Figures 12a and 12c.

The driving force for these changes is increased surface flow at high elevations, as infiltration excess produced from Noah-MP that would otherwise be removed from the system as a sink is allowed to flow down-gradient through WRF-Hydro. Table 5 also shows that soil moisture and ET increase the most at lower elevations, which is expected since increased surface runoff results in more infiltration further downstream in the basin. This occurs to a lesser extent at higher elevations.

## 5. Summary and Implications

This article presents the development of the coupled LIS/WRF-Hydro system, which is aimed at exploiting and connecting the land surface DA capabilities of NASA LIS and the hydrological modeling capabilities of WRF-Hydro. The coupled environment is facilitated using the constructs of the ESMF, enabling a flexible and interoperable environment that integrates the two large modeling systems. The application of the coupled LIS/WRF-Hydro system is demonstrated over the Tuolumne basin in California, where remotely sensed SWE estimates from the NASA ASO data set are employed for DA. The ASO SWE estimates are assimilated within LIS to improve the representation of snow states within the land surface model, and the coupled LIS/WRF-Hydro environment is used to examine the corresponding impacts on streamflow from snow DA. The ASO estimates are



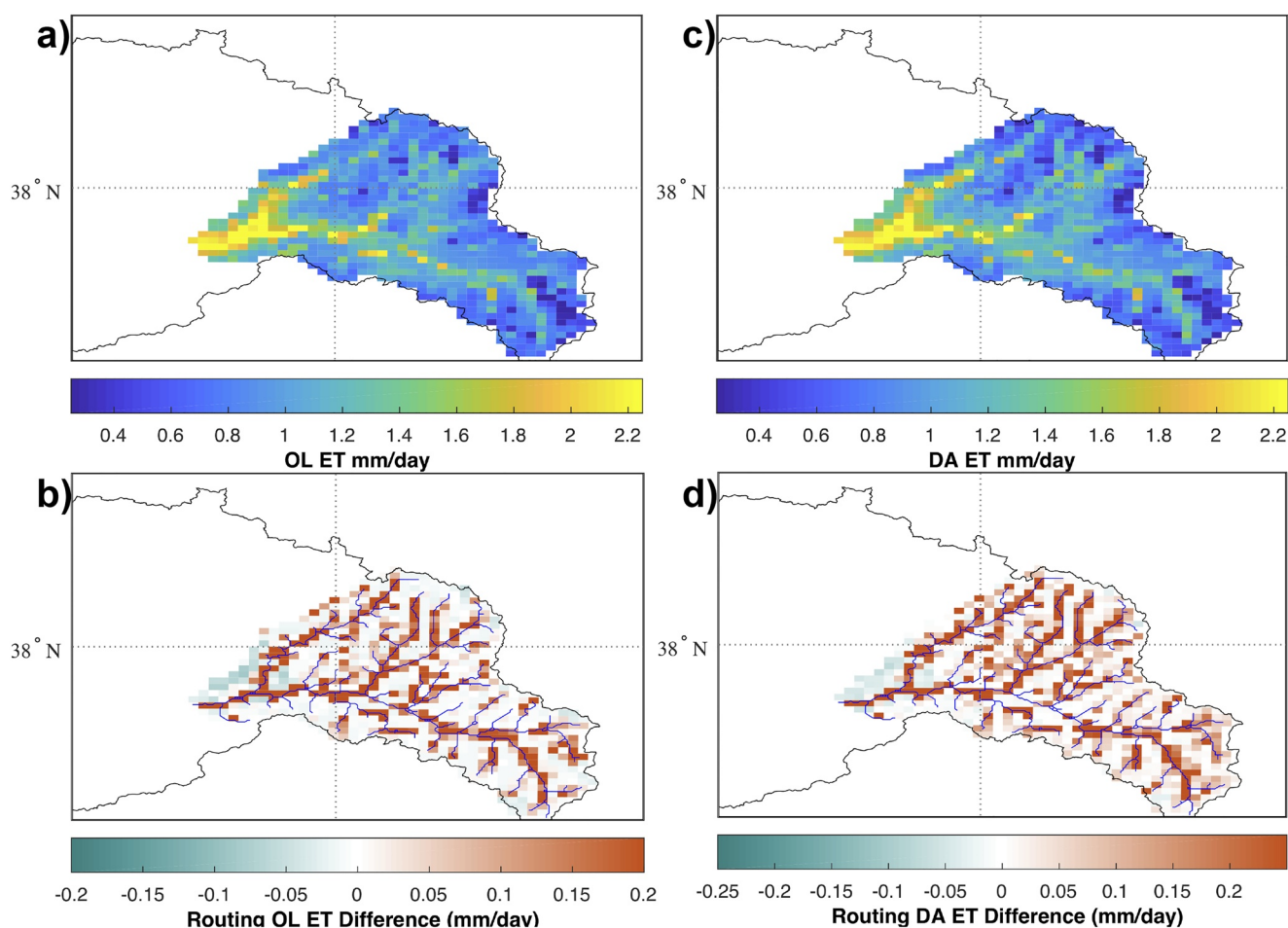


**Figure 12.** Average ET (mm/day) for LIS/WRF-Hydro (top) and change in ET in LIS/WRF-Hydro compared to LIS (bottom) for the OL (left) and DA (right) simulations.

available over a subset of the entire modeled domain. For this work, we use EnKF DA due to its ability to run with fewer ensembles and its shorter latency window, which is ideal for a streamflow forecasting proof of concept. This would not preclude the use of other DA methods such as particle smoothing (e.g., Margulis et al., 2019) for future work if the computational challenge of its larger ensemble size could be overcome.

Over areas where ASO coverage exist, the ASO SWE DA leads to reduced SWE biases (Table 3) in the LIS/WRF-Hydro simulations. Further, these benefits also extend to the hydrologic model simulation through the improvements to model runoff. For example, streamflow bias at USGS gauge 11274790 (above Hetch Hetchy Reservoir) is reduced from 16% to less than 10% with DA. The benefits of snow DA for streamflow are better understood when considering the impacts of DA on surface runoff entering channels (i.e., Figure 10), as removal of snow at low elevations tends to reduce high bias during wet years, while added snow at high elevations tends to reduce negative bias during dry years.

Model improvements via reductions of model streamflow biases above Hetch Hetchy reservoir from ASO DA (too dry in dry years and too wet in wet years) should be significant for water management in the western US and other semi-arid environments with growing populations. We also note that negative SWE bias is reduced across much of the high-elevation northern area of the study region, while excess SWE in the valleys and at generally

**Table 5**

*Average Percent Increase to ET and Soil Moisture Between LIS/WRF-Hydro and LIS (LIS/WRF-Hydro – LIS) for Elevation Ranges Across the Upper Basin Model Analysis Domain (Figure 2)*

Elevation Range (m)	ET (%-Increase)	0–10 cm Soil Vol. Water (%-Increase)
1,400–1,800	8.83	4.80
1,800–2,200	11.63	4.62
2,200–2,600	8.47	3.13
2,600–3,000	8.53	2.91
3,000–3,400	8.61	2.28
3,400–3,800	5.17	2.33

*Note.* Analysis is for simulations with DA.

lower elevations is removed. At high elevations, especially to the North, SWE is increased by over 60% in some areas, while it is reduced by ~25% in lower elevations (Figure 3). This redistribution of SWE with additional SWE in the headwaters and reduced SWE downstream improves the hydrologic response, where the former reduces negative bias during dry years and the latter reduces excessive positive bias of streamflow above Hetch Hetchy Reservoir during wet years. If SWE DA in hydrologic models can improve forecasts of streamflow entering reservoirs, this modeling framework (applied in a real-time quasi-operational simulation) could potentially be significant for dam operations and seasonal water forecasts.

Addressing the impacts of SWE DA on streamflow for this application would not be possible without the integrated capabilities of LIS coupled to WRF-Hydro. Though prior studies have examined the use of remote sensing snow measurements on land surface characterization, only a few studies have focused their impact on the integrated land and hydrological response (e.g., Caleb & Moradkhani, 2011; Huang et al., 2017; Liu et al., 2015). The results described here therefore provide the systematic process level quantification of the impact of ASO SWE DA on various land surface and hydrologic processes. As future remote sensing estimates of snow are being developed, quantitative assessment of their anticipated utility for hydrologic process improvements is important to quantify. The methodology and the results of this study using the coupled LIS/WRF-Hydro system serve as an important benchmark in this regard.

The evaluations presented in this study also indicate that the systematic errors in the snow and streamflow estimates are significant sources of uncertainty in the model simulations. These errors may be due to uncertainties in model forcing, physics schemes within the model structure, and adjustable parameters. To further improve the accuracy of model simulations (including those with DA), calibration (e.g., Gupta et al., 2009; Samaniego et al., 2010) of land surface and hydrologic parameters that control surface water partitioning, snow, and flow routing parameters could be beneficial. The calibration approaches must also consider inconsistencies between model streamflow and surface variables, as Lahmers et al. (2019) demonstrated that calibration to surface flow degraded soil moisture in some southwest US catchments. Both LIS and WRF-Hydro include significant parameter estimation capabilities, which could be exploited to potentially ameliorate these issues through the refinement of relevant model parameters.

Another finding of this analysis is the coupled LIS/WRF-Hydro system simulates the redistribution of soil moisture from the feedback of the hydrologic model into the land surface model. Over the simulation domain, this feedback leads to increases in soil moisture and ET in areas near the channel network. ET and soil moisture near the channel network can increase by over 10% in some locations (Figures 11 and 12). These findings are similar to the results from Lahmers et al. (2020), who showed that soil moisture increases in WRF-Hydro compared to control simulations without surface hydrology in a semi-arid environment, especially in areas with low soil conductivity. This addition of physical processes representing surface hydrology can therefore impact land-atmosphere interactions in some environments (e.g., Lahmers et al., 2020), and is thus relevant to future work.

The combination of DA and hydrologic routing in the coupled LIS/WRF-Hydro modeling system opens up new possibilities for the analysis of surface processes on atmospheric coupling (e.g., Santanello et al., 2018). The snow DA example demonstrated here is a “weakly coupled” DA instance where the assimilation is performed within the offline land surface model and the impacts on streamflow are demonstrated (indirectly) through the mediator between LIS and WRF-Hydro. The development of the coupled system also paves the way for strongly coupled DA environments where cross-model DA updates are used. For example, the assimilation of streamflow observations within WRF-Hydro could be employed with the land surface moisture variables (in LIS) updated in a DA instance. Such a strongly coupled DA environment could be accomplished with an additional mediator designed specifically for DA related exchanges. Similarly, the addition of hydrologic routing and its impacts on soil moisture could influence surface fluxes, as was shown in previous literature (e.g., Arnault et al., 2016; Lahmers et al., 2020; Maxwell et al., 2011). Thus, this new coupled modeling system has the potential to combine both of these abilities to improve our understanding of land surface processes and variables on atmospheric processes that govern NWP and climate prediction.

## Data Availability Statement

The LIS/WRF-Hydro model is available online as the NASA-Land-Coupler: <https://github.com/NASA-LIS/NASA-Land-Coupler.git>. The version of LIS/WRF-Hydro used for this manuscript is tagged online at: <https://github.com/NASA-LIS/NASA-Land-Coupler/tree/96017ce6dbf4783efa4e22a6d9b2d7b40ef10960/src>.

Archived plotting scripts and post-processed data are available for download at: <https://doi.org/10.5281/zenodo.6330018>. ASO snow data are available online at: <https://nsidc.org/data/aso>. California Department of Water Resources Data are available at: <https://cdec.water.ca.gov/snow/current/snow/>. SNODAS data are available at: <https://nsidc.org/data/g02158>, and University of Arizona SWE data are available at: <https://nsidc.org/data/nsidc-0719/versions/1>. NLDAS-2 forcing data are available at: [https://disc.sci.gsfc.nasa.gov/datasets/NLDAS\\_NOAH0125\\_H\\_002/summary?keywords=NLDAS](https://disc.sci.gsfc.nasa.gov/datasets/NLDAS_NOAH0125_H_002/summary?keywords=NLDAS). USGS streamflow data were downloaded using the USGS data retrieval tools (available at: <https://owi.usgs.gov/R/training-curriculum/usgs-packages/dataRetrieval-readN-WIS/>) with data stored at: <https://waterservices.usgs.gov/>.

## Acknowledgments

This work was supported by NASA Modeling, Analysis, and Prediction (MAP) Federal Grant Number: NNN15ZDA001N-MAP and by the NASA Postdoctoral Program (NPP).

## References

- Anderson, E. A. (1973). National Weather Service River Forecast System – Snow Accumulation and Ablation Model. *NOAA Technical Memorandum: NWS Hydro-17*. US National Weather Service.
- Arnault, J., Wagner, S., Rummeler, T., Fersch, B., Bliefernicht, J., Andresen, S., & Kunstmann, H. (2016). Role of runoff–infiltration partitioning and resolved overland flow on land–Atmosphere feedbacks: A case study with the WRF-hydro coupled modeling system for West Africa. *Journal of Hydrometeorology*, 17, 1489–1516. <https://doi.org/10.1175/jhm-d-15-0089.1>
- Arsenault, K. R., Kumar, S. V., Geiger, J. V., Wang, S., Kemp, E., Mocko, D. M., et al. (2018). The Land surface Data Toolkit (LDT v7.2) – A data fusion environment for land data assimilation systems. *Geoscientific Model Development*, 11, 3605–3621. <https://doi.org/10.5194/gmd-11-3605-2018>
- Barbu, A. L., Calvet, J.-C., Mahfouf, J.-F., & Lafont, S. (2014). Integrating ASCAT surface soil moisture and GEOV1 leaf area index into the SURFEX modelling platform: A land data assimilation application over France. *Hydrol. Journal of Earth System Science*, 118, 173–192. <https://doi.org/10.5194/hess-18-173-2014>
- Barrett, A. (2003). National Operational Hydrologic Remote Sensing Center SNOw Data Assimilation System (SNODAS) Products at NSIDC. *NSIDC Special Report 11*. National Snow and Ice Data Center Digital Media.
- Caleb, D., & Moradkhani, H. (2011). Radiance data assimilation for operational snow and streamflow forecasting. *Advances in Water Resources*, 34(3), 351–364.
- Cao, Q., Painter, T. H., Curriet, W. R., Lundquist, J. D., & Lettenmaier, D. P. (2018). Estimation of precipitation over the OLYMPLEX domain during Winter 2015/16. *Journal of Hydrometeorology*, 19, 143–160. <https://doi.org/10.1175/JHM-D-17-0076.1>
- Clark, M. P., Bierkens, M. F. P., Samaniego, L., Woods, R. A., Uijlenhoet, R., Bennett, K. E., et al. (2017). The evolution of process-based hydrologic models: Historical challenges and the collective quest for physical realism. *Hydrology and Earth System Sciences*, 21, 3427–3440. <https://doi.org/10.5194/hess-21-3427-2017>
- Clark, M. P., Fan, Y., Lawrence, D. M., Adam, J. C., Bolster, D., Gochis, D. J., et al. (2015). Improving the representation of hydrologic processes in Earth System Models. *Water Resources Research*, 51, 5929–5956. <https://doi.org/10.1002/2015WR017096>
- Crow, W. T., & Van Loon, E. (2006). Impact of Incorrect Model Error Assumptions on the Sequential Assimilation of Remotely Sensed Surface Soil Moisture. *Journal of Hydrometeorology*, 7(3), 421–432. <https://doi.org/10.1175/jhm499.1>
- Dawson, N., Broxton, P., Zeng, X., Leuthold, M., Barlage, M., & Holbrook, P. (2016). An evaluation of snow initializations in NCEP global and regional forecasting models. *Journal of Hydrometeorology*, 17(6), 1885–1901. <https://doi.org/10.1175/jhm-d-15-0227.1>
- de Lannoy, G. J. M., Reichle, R. H., Arsenault, K. R., Houser, P. R., Kumar, S., Verhoest, N. E. C., & Pauwels, V. R. N. (2012). Multiscale assimilation of advanced microwave scanning radiometer–EOS snow water equivalent and moderate resolution imaging spectroradiometer snow cover fraction observations in northern Colorado. *Water Resources Research*, 48, W01522. <https://doi.org/10.1029/2011wr010588>
- Ek, M. B., Mitchell, K. E., Lin, Y., Rogers, E., Grunmann, P., Koren, V., et al. (2003). Implementation of Noah land surface model advances in the National Centers for Environmental Prediction operational mesoscale Eta model. *Journal of Geophysical Research*, 108, 8851. <https://doi.org/10.1029/2002JD003296>
- Gochis, D. J., Barlage, M., Cabell, R., Casali, M., Dugger, A., FitzGerald, K., et al. (2020). The WRF-Hydro(R) modeling system technical description, (Version 5.1.1). *NCAR Technical Note*. <https://doi.org/10.5281/zenodo.3625238>
- Gupta, H. V., Kling, H., Yilmaz, K., & Martinez, G. (2009). Decomposition of the mean squared error and NSE performance criteria: Implications for improving hydrological modeling. *Journal of Hydrology*, 377, 80–91. <https://doi.org/10.1016/j.jhydrol.2009.08.003>
- Hain, C. R., Crow, W. T., Anderson, M. C., & Mecikalski, J. R. (2012). An ensemble Kalman filter dual assimilation of thermal infrared and microwave satellite observations of soil moisture into the Noah land surface model. *Water Resources Research*, 48, W11517. <https://doi.org/10.1029/2011WR011268>
- Hamman, J. J., Nijssen, B., Bohn, T. J., Gergel, D. R., & Mao, Y. (2018). The variable infiltration capacity model version 5 (VIC-5): Infrastructure improvements for new applications and reproducibility. *Geoscientific Model Development*, 11, 3481–3496. <https://doi.org/10.5194/gmd-11-3481-2018>
- Henn, B., Clark, M. P., Kavetski, D., McGurk, B., Painter, T. H., & Lundquist, J. D. (2016). Combining snow, streamflow, and precipitation gauge observations to infer basin-mean precipitation. *Water Resources Research*, 52, 8700–8723. <https://doi.org/10.1002/2015WR018564>
- Hill, C., DeLuca, C., Balaji, V., Suarez, M., & da Silva, A. (2004). Architecture of the Earth. *System Modeling Framework*. IEEE Computational Science and Engineering, 6(1), 18–28.
- Houtekamer, P. L., & Mitchell, H. L. (1998). Data assimilation using an ensemble kalman filter technique. *Monthly Weather Review* (Vol. 126, pp. 7962–8811). CO. [https://doi.org/10.1175/1520-0493\(1998\)126<0796:dauaek>2.0.co;2](https://doi.org/10.1175/1520-0493(1998)126<0796:dauaek>2.0.co;2)
- Huang, C., Newman, A. J., Clark, M. P., Wood, A. W., & Zheng, X. (2017). Evaluation of snow data assimilation using the ensemble Kalman filter for seasonal streamflow prediction in the Western United States. *Hydrology and Earth System Sciences*, 21, 635–650. <https://doi.org/10.5194/hess-21-635-2017>
- Julien, P. Y., Saghaian, B., & Ogden, F. L. (1995). Raster-based hydrological modeling of spatially-varied surface runoff. *Journal of the American Water Resources Association*, 31, 523–536. <https://doi.org/10.1111/j.1752-1688.1995.tb04039.x>
- Kumar, S., Reichle, R., Koster, R., Crow, W., & Peters-Lidard, C. (2009). Role of subsurface physics in the assimilation of surface soil moisture observations. *Journal of Hydrometeorology*, 10, 1534–1547. <https://doi.org/10.1175/2009JHM1134.1>
- Kumar, S. V., Dong, J., Peters-Lidard, C. D., Mocko, D., & Gómez, B. (2017). Role of forcing uncertainty and background model error characterization in snow data assimilation. *Hydrology and Earth System Sciences*, 21, 2637–2647. <https://doi.org/10.5194/hess-21-2637-2017>

- Kumar, S. V., Holmes, T. R., Bindlish, R., de Jeu, R., & Peters-Lidard, C. D. (2020). Assimilation of vegetation optical depth retrievals from passive microwave radiometry. *Hydrology and Earth System Sciences*, 24, 1–20. <https://doi.org/10.5194/hess-24-3431-2020>
- Kumar, S. V., Jasinski, M., Mocko, D. M., Rodell, M., Borak, J., Li, B., et al. (2019a). NCA-LDAS land analysis: Development and performance of a multisensor, multivariate land data assimilation system for the National Climate Assessment. *Journal of Hydrometeorology*, 20, 1571–1593. <https://doi.org/10.1175/jhm-d-17-0125.1>
- Kumar, S. V., Mocko, D. M., Wang, S., Peters-Lidard, C. D., & Borak, J. (2019b). Assimilation of remotely sensed Leaf Area Index into the Noah-MP land surface model: Impacts on water and carbon fluxes and states over the Continental U.S. *Journal of Hydrometeorology*, 20, 1359–1377. <https://doi.org/10.1175/jhm-d-18-0237.1>
- Kumar, S. V., Peters-Lidard, C. D., Arsenault, K. R., Getirana, A., Mocko, D., & Liu, Y. (2015a). Quantifying the added value of snow cover area observations in passive microwave snow depth assimilation. *Journal of Hydrometeorology*, 16(4), 1736–1741. <https://doi.org/10.1175/JHM-D-15-0021.1>
- Kumar, S. V., Peters-Lidard, C. D., Mocko, D., Reichle, R., Liu, Y., Arsenault, K. R., et al. (2014). Assimilation of remotely sensed soil moisture and snow depth retrievals for drought estimation. *Journal of Hydrometeorology*, 15, 2446–2469. <https://doi.org/10.1175/jhm-d-13-0132.1>
- Kumar, S. V., Peters-Lidard, C. D., Santanello, J. A., Reichle, R. H., Draper, C. S., Koster, R. D., et al. (2015b). Evaluating the utility of satellite soil moisture retrievals over irrigated areas and the ability of land data assimilation methods to correct for unmodeled processes. *Hydrology and Earth System Sciences*, 19, 4463–4478. <https://doi.org/10.5194/hess-19-4463-2015>
- Kumar, S. V., Peters-Lidard, C. D., Tian, Y., Houser, P., Geiger, J., Olden, S., et al. (2006). Land Information System - An interoperable framework for high resolution land surface modeling. *Environmental Modelling & Software*, 21, 1402–1415. <https://doi.org/10.1016/j.envsoft.2005.07.004>
- Kumar, S. V., Reichle, R. H., Peters-Lidard, C. D., Koster, R. D., Zhan, X., Crow, W. T., et al. (2008). A land surface data assimilation framework using the Land Information System: Description and applications. *Advances in Water Resources*, 31, 1419–1432. <https://doi.org/10.1016/j.advwatres.2008.01.013>
- Kumar, S. V., Zaitchik, B. F., Peters-Lidard, C. D., Rodell, M., Reichle, R., Li, B., et al. (2016). Assimilation of gridded GRACE terrestrial water storage estimates in the North American Land Data Assimilation System (NLDAS). *Journal of Hydrometeorology*, 17(7), 1951–1972. <https://doi.org/10.1175/JHM-D-15-0157.1>
- Lahmers, T. M., Castro, C. L., & Hazenberg, P. (2020). Effects of lateral flow on the convective environment in a coupled hydrometeorological modeling system in a semiarid environment. *Journal of Hydrometeorology*, 21, 615–642. <https://doi.org/10.1175/jhm-d-19-0100.1>
- Lahmers, T. M., Gupta, H., Castro, C. L., Gochis, D. J., Yates, D., Dugger, A., et al. (2019). Enhancing the Structure of the WRF-Hydro Hydrologic Model for Semiarid Environments. *Journal of Hydrometeorology*, 20, 691–714. <https://doi.org/10.1175/jhm-d-18-0064.1>
- Lahmers, T. M., Hazenberg, P., Gupta, H. V., Castro, C. L., Gochis, D. J., Dugger, A. L., et al. (2021). Evaluation of NOAA national water model parameter calibration in semi-arid environments prone to channel infiltration. *Journal of Hydrometeorology*. <https://doi.org/10.1175/JHM-D-20-0198.1>
- Lettenmaier, D. P., Alsdorf, D., Dozier, J., Huffman, G. J., Pan, M., & Wood, E. F. (2015). Inroads of remote sensing into hydrologic science during the WRR era. *Water Resources Research*, 51, 7309–7342. <https://doi.org/10.1002/2015WR017616>
- Liu, Y., Peters-Lidard, C. D., Kumar, S. V., Arsenault, K., & Mocko, D. (2015). Blending satellite based snow depth products with in-situ observations for streamflow predictions in the upper Colorado River basin. *Water Resources Research*. <https://doi.org/10.1002/2014WR016606>
- Liu, Y., Peters-Lidard, C. D., Kumar, S. V., Foster, J. L., Shaw, M., Tian, Y., & Fall, G. M. (2013). Assimilating satellite-based snow depth and snow cover products for improving snow predictions in Alaska. *Advances in Water Resources*, 54, 208–227. <https://doi.org/10.1016/j.advwatres.2013.02.005>
- Margulis, S. A., Fang, Y., Li, D., Lettenmaier, D. P., & Andreadis, K. (2019). The utility of infrequent snow depth images for deriving continuous space-time estimates of seasonal snow water equivalent. *Geophysical Research Letters*, 46(10), 5331–5340. <https://doi.org/10.1029/2019gl082507>
- Maxwell, R. M., Lundquist, J. K., Mirocha, J. D., Smith, S. G., Woodward, C. S., & Tompson, A. F. B. (2011). Development of a Coupled Groundwater–Atmosphere Model. *Monthly Weather Review*, 139, 96–116. <https://doi.org/10.1175/2010mwr3392.1>
- Nerini, D., Foresti, L., Leuenberger, D., Robert, S., & Germann, U. (2019). A reduced-space ensemble kalman filter approach for flow-dependent integration of radar extrapolation nowcasts and NWP precipitation ensembles. *Monthly Weather Review*, 147(3), 987–1006. <https://doi.org/10.1175/MWR-D-18-0258.1>
- Nielsen, S. A., & Hansen, E. (1973). Numerical simulation of the rainfall runoff process on a daily basis. *Nordic Hydrology*, 4, 171–190. <https://doi.org/10.2166/nh.1973.0013>
- Niu, G. Y., Yang, Z. L., Mitchell, K. E., Chen, F., Ek, M. B., Barlage, M., et al. (2011). The community Noah land surface model with multiparameterization options (Noah-MP): 1. Model description and evaluation with local-scale measurements. *Journal of Geophysical Research*, 116. <https://doi.org/10.1029/2010jd015139>
- Oaida, C. M., Reager, J. T., Andreadis, K. M., David, C. H., Levoe, S. R., Painter, T. H., et al. (2019). A high-resolution data assimilation framework for snow water equivalent estimation across the Western United States and validation with the airborne snow observatory. *Journal of Hydrometeorology*, 20, 357–378. <https://doi.org/10.1175/JHM-D-18-0009.1>
- Ogden, F. L. (1997). *CASC2D Reference Manual* (p. 106). Dept. of Civil and Environmental Engineering U-37, University of Connecticut.
- Painter, T. H., Berisford, D. F., Boardman, J. W., Bormann, K. J., Deems, J. S., Gehrke, F., et al. (2016). The Airborne Snow Observatory: Fusion of scanning lidar, imaging spectrometer, and physically-based modeling for mapping snow water equivalent and snow albedo. *Remote Sensing of Environment*, 184, 139–152. <https://doi.org/10.1016/j.rse.2016.06.018>
- Painter, T. H., Rittger, K., McKenzie, C., Slaughter, P., Davis, R. E., & Dozier, J. (2009). Retrieval of subpixel snow-covered area, grain size, and albedo from MODIS. *Remote Sensing of Environment*, 113, 868–879. <https://doi.org/10.1016/j.rse.2009.01.001>
- Pan, M., & Wood, E. F. (2006). Data assimilation for estimating the terrestrial water budget using a constrained ensemble kalman filter. *Journal of Hydrometeorology*, 7(3), 534–547. <https://doi.org/10.1175/jhm495.1>
- Peters-Lidard, C. D., Clark, M., Samaniego, L., Verhoest, N. E. C., van Emmerik, T., Uijlenhoet, R., et al. (2017). Scaling, similarity, and the fourth paradigm for hydrology. *Journal of Earth System Science*, 21, 3701–3713. <https://doi.org/10.5194/hess-21-3701-2017>
- Peters-Lidard, C. D., Houser, P. R., Tian, Y., Kumar, S. V., Geiger, J., Olden, S., et al. (2007). High-performance Earth system modeling with NASA/GSFC's Land Information System. *Innovations in Systems and Software Engineering*, 3(3), 157–165. <https://doi.org/10.1007/s11334-007-0028-x>
- Peters-Lidard, C. D., Kumar, S. V., Mocko, D., & Tian, Y. (2011). Estimating evapotranspiration with land data assimilation systems. *Hydrological Processes*, 25(26), 3979–3992. <https://doi.org/10.1002/hyp.8387>
- Pitman, A. J. (2003). The evolution of, and revolution in, land surface schemes designed for climate models. *International Journal of Climatology*, 23, 479–510. <https://doi.org/10.1002/joc.893>



- Regan, R. S., Markstrom, S. L., & LaFontaine, J. H. (2020). *PRMS version 5.1.0: Precipitation-Runoff Modeling System (PRMS): U.S. Geological Survey Software Release*.
- Reichle, R., Koster, R. D., Liu, P., Mahanama, S. P. P., Njoku, E. G., & Owe, M. (2007). Comparison and assimilation of global soil moisture retrievals from the Advanced Microwave Scanning Radiometer for the Earth Observing System (AMSR-E) and the Scanning Multichannel Microwave Radiometer (SMMR). *Journal of Geophysical Research*, 112, D09108. <https://doi.org/10.1029/2006jd008033>
- Reichle, R. H., Crow, W. T., & Keppenne, C. L. (2008). An adaptive ensemble Kalman filter for soil moisture data assimilation. *Water Resources Research*, 44, W03423. <https://doi.org/10.1029/2007WR006357>
- Reichle, R. H., Kumar, S. V., Mahanama, S. P. P., Koster, R. D., & Liu, Q. (2010). Assimilation of satellite-derived skin temperature observations into land surface models. *Journal of Hydrometeorology*, 11(5), 1103–1122. <https://doi.org/10.1175/2010JHM1262.1>
- Reichle, R. H., McLaughlin, D. B., & Entekhabi, D. (2002). Hydrologic Data Assimilation with the Ensemble Kalman Filter. *Monthly Weather Review*, 130(1), 103–114. [https://doi.org/10.1175/1520-0493\(2002\)130<0103:hdawte>2.0.co;2](https://doi.org/10.1175/1520-0493(2002)130<0103:hdawte>2.0.co;2)
- Ryu, D., Crow, W. T., Zhan, X., & Jackson, T. J. (2009). Correcting unintended perturbation biases in hydrologic data assimilation. *Journal of Hydrometeorology*, 10(3), 734–750. <https://doi.org/10.1175/2008jhm1038.1>
- Samaniego, L., Kumar, R., & Attinger, S. (2010). Multiscale parameter regionalization of a grid-based hydrologic model at the mesoscale. *Water Resources Research*, 46, W05523. <https://doi.org/10.1029/2008WR007327>
- Sampson, K., & Gochis, D. J. (2020). *WRF Hydro GIS Pre-Processing Tools* (p. 45). Retrieved from [https://github.com/NCAR/wrf\\_hydro\\_arcgis\\_preprocessor/releases/download/v5.1.1/WRFHydro\\_GIS\\_Preprocessor\\_v5\\_1\\_1.pdf](https://github.com/NCAR/wrf_hydro_arcgis_preprocessor/releases/download/v5.1.1/WRFHydro_GIS_Preprocessor_v5_1_1.pdf)
- Santanello, J. A., Dirmeyer, P. A., Ferguson, C. R., Findell, K. L., Tawfik, A. B., Berg, A., et al. (2018). Land–Atmosphere Interactions: The LoCo Perspective. *Bulletin of the American Meteorological Society*, 99, 1253–1272. <https://doi.org/10.1175/bams-d-17-0001.1>
- Su, H., Yang, Z.-L., Dickinson, R. E., Wilson, C. R., & Niu, G.-Y. (2011). Multisensor snow data assimilation at the continental scale: The value of gravity recovery and climate experiment terrestrial water storage information. *Journal of Geophysical Research*, 115(D10), 1–14. <https://doi.org/10.1029/2009JD013035>
- Sun, N., Wigmosta, M., Zhou, T., Lundquist, J., Dickerson-Lange, S., & Cristea, N. (2018). Evaluating the functionality and streamflow impacts of explicitly modelling forest–Snow interactions and canopy gaps in a distributed hydrologic model. *Hydrological Processes*, 32(13), 2128–2140. <https://doi.org/10.1002/hyp.13150>
- Theurich (2014). NUOPC Layer Reference, ESMF v7.0.0. Retrieved from <https://www.earthsystemcog.org/projects/nuopc/refmans>
- Xia, Y., Mitchell, K., Ek, M., Sheffield, J., Cosgrove, B., Wood, E., et al. (2012). Continental-scale water and energy flux analysis and validation for the North American Land Data Assimilation System project phase 2 (NLDAS-2): 1. Intercomparison and application of model products. *Journal of Geophysical Research*, 117, D03109. <https://doi.org/10.1029/2011JD016048>
- Zaitchik, B. F., & Rodell, M. (2009). Forward-looking assimilation of MODIS-derived snow-covered area into a land surface model. *Journal of Hydrometeorology*, 10, 130–148. <https://doi.org/10.1175/2008jhm1042.1>
- Zhou, Y., McLaughlin, D., & Entekhabi, D. (2006). Assessing the performance of the ensemble kalman filter for land surface data assimilation. *Monthly Weather Review*, 134(8), 2128–2142. <https://doi.org/10.1175/mwr3153.1>